School of Physics and Astronomy

Rapid Parameterization and Estimated Inclination of Gravitational Waves from Binary Systems

S. A. Usman

Submitted for the degree of Master of Philosophy
School of Physics and Astronomy
Cardiff University

August 2018

Declaration of Authorship

- DECLARATION:
  This work has not been submitted in substance for any other degree or award at this or any other university or place of learning, nor is being submitted concurrently in candidature for any degree or other award.

  Signed: .... (candidate) Date: ....

- STATEMENT 1:
  This thesis is being submitted in partial fulfillment of the requirements for the degree of Master of Philosophy (MPhil).

  Signed: .... (candidate) Date: ....

- STATEMENT 2:
  This thesis is the result of my own independent work/investigation, except where otherwise stated. Other sources are acknowledged by explicit references. The views expressed are my own.

  Signed: .... (candidate) Date: ....

- STATEMENT 3:
  I hereby give consent for my thesis, if accepted, to be available for photocopying and for inter-library loan, and for the title and summary to be made available to outside organisations.

  Signed: .... (candidate) Date: ....

- STATEMENT 4: PREVIOUSLY APPROVED BAR ON ACCESS
  I hereby give consent for my thesis, if accepted, to be available for photocopying and for inter-library loans **after expiry of a bar on access previously approved by the Academic Standards & Quality Committee.**

  Signed: .... (candidate) Date: ....

Summary of Thesis

The Laser Interferometer Gravitational-Wave Observatory (LIGO) has successfully started the era of gravitational-wave astronomy with its groundbreaking detections of gravitational waves. These signals have opened the door to a new way to listen to the universe. The detections have already taught us much about the universe. Firstly, the detection of gravitational waves confirms a key prediction of Einstein's theory of General Relativity. LIGO has also given more information on binary black hole populations and has confirmed that short gamma-ray bursts can be generated by binary neutron star mergers. In Chapter 1, I explore the basic premises of gravitational waves, their sources and the detectors that find them. I then explain how we identify the signals in our data in Chapter 3.

We hope to maximize the information we can learn from LIGO's detections. In order to do that, we need to extract as much information about the sources as possible from the gravitational waves. For example, by measuring the distance of black hole binaries accurately, some have suggested constraining the Hubble constant H_0 after multiple measurments. In Chapter 2, I explore the degeneracy between inclination and distance and LIGO's ability to constrain the distance and inclination from binary systems. We find that even with detectors sensitive to both polarizations of gravitational waves, LIGO would be unable to differentiate a signal from a nearby, inclined system or a far-away, face-on system, without breaking the degeneracy using measurements from electromagnetic signals (for binary neutron star systems), precession (for highly spinning objects) or higher modes (for high mass-ratio systems).

Additionally, it may be beneficial to measure the parameters of binary systems quickly, especially when there is the chance of detecting an associated electromagnetic signature, as is the case with binary neutron star systems and neutron star-black hole binaries. For this reason, I begin to build a case for a new method of rapid parameter estimation in Chapter 4.

"Your goal today should be to be better tomorrow than you are today."

—Jeremy Arel

Contents

Co-authored Papers and Results Disclaimer

Some sections of this thesis include co-authored work which has previously been published, in addition to pieces of work which are currently under internal review before publication.

- Chapter 2 presents research on LIGO's inability to measure the inclination of a binary system using gravitational waves alone. This chapter's results are discussed in the forthcoming paper "Constraining the Inclination of Binary Mergers from Gravitational Wave Observations". Samantha Usman is lead author of this paper.

- Chapter 3 presents an overview of LIGO's offline search pipeline. This is a summary of "The PyCBC search for gravitational waves from compact binary coalescence" [24]. This research was completed prior to research conducted in this thesis. Samantha Usman is the lead author of this paper.

Chapter 1

Gravitational Waves: Theory, Sources, and Detectors

1.1 Introduction

On September 14th, 2015, the Laser Interferometer Gravitational-Wave Observatory (LIGO) [1, 2] and Virgo made a mark on history by directly observing a gravitational wave for the first time [3]. This event signified the beginning of gravitational-wave astronomy, an entirely new way to interpret our universe. The LIGO-Virgo Collaboration has since observed several more gravitational-wave signals from binary black hole systems [4, 5, 6, 7] as well as a gravitational-wave from a binary neutron star system and its associated electromagnetic counterpart [8, 9].

The binary black hole detections provide the first evidence of a new population of black holes, whose masses are larger than what had been seen in X-ray studies [10]. With accurate estimates of their distance, the binary black hole detections have been theorized to be able to constrain the Hubble constant [11]. With more binary neutron star detections, astronomers may be able to constrain the nuclear equation of state [12]. These gravitational waves are thus significant for both detecting a phenomenon which had never before been directly observed and the technical advances necessary to make such an observation, as well as the advances in astrophysical knowledge that this fledgling branch of astronomy promises.

1.1.1 What are gravitational waves?

When Newton first described gravity, he described it as an inherent and unexplainable force that drew two objects toward each other [13]. This force was described to effect everything that has mass and would be stronger the more massive and the closer two objects were. This is summarized by Newton's law of gravitation: $F = \frac{Gm_1m_2}{r^2}$. Here, f is the force between two objects of mass m_1 and m_2 separated by a distance r. G represents the gravitational constant. This law was extremely useful and could be applied in all practical applications. However, the law could not explain the underlying mechanism of the force, and in some cases, such as the Mercury's perhelion precession, did not quite fit to observations [14]. Similarly behavior has recently been observed in the star S2 orbiting black hole candidate Sagittarius A* [15].

When Einstein published his theory of general relativity in 1918, he put forward a new understanding of gravity: his theory suggested that mass curved space, and what we observe to be gravity is the natural path of objects moving in curved space [16]. This theory brought with it a suprising result: the equation describing the fabric of space and time had a wave solution. This meant it was possible to create wave-like properties in the fabric of space itself. This phenomenon came to be called gravitational waves [17].

Looking at the result of gravitational waves, several things could be inferred: one, gravitational waves are generated whenever there is a changing quadrupole moment, i.e. whenever there is accelerating mass. However, it would be extremely hard to detect the effect of these gravitational waves in a laboratory, since, two, gravitational waves are very weak. Mass and spacetime couple extremely weakly, so in order to detect gravitational waves, we must use extremely massive objects moving at very high speeds. For this reason, we look to astrophysical sources.

The resulting gravitational waves would stretch and skew space perpendicular to its direction of travel. In addition, like electromagnetic radiation, the waves travel at the speed of light, and there are only two possible polarizations for a given gravitational wave in General Relativity. These polarizations are called the plus (+) and cross (×) polarizations, since they bend space along a plus and cross orientation, as seen in Figure 1.1. Once these basic properties are established, the next question is: how would we be able to measure the effect of these gravitational waves? This is where the LIGO and Virgo detectors step in.
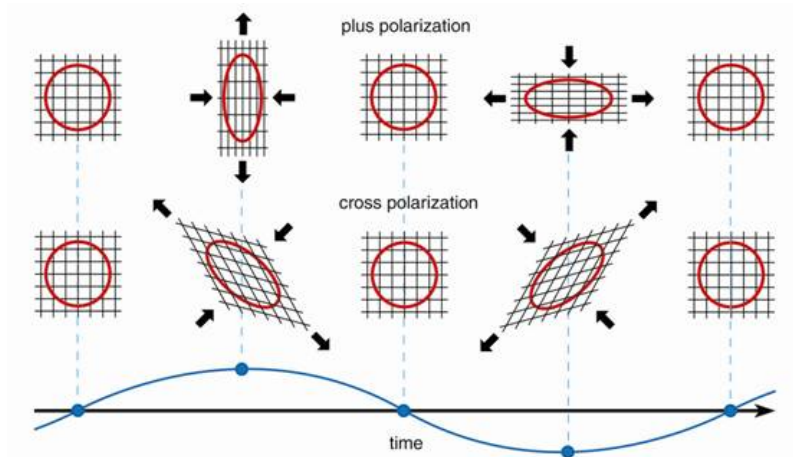
Figure 1.1: The effect of a plus or cross polarization of a gravitational wave on a ring of particles as it passes through space, (in the direction in or out of the page). Image from [18].

1.2 How do the detectors work?

Since gravitational waves stretch and skew the fabric of space, we would need essentially a high-tech ruler which would be able to notice minute changes in the length of space to detect them. The difficulty lies in the fact that any bend in the fabric of space will also affect any object occupying that space. For this reason, we turn to light itself to measure the length of space. Light can measure distance by timing how long it takes to travel between two objects. If the objects have not moved, and it takes more time to travel between them than it had previously, we know that the length of space between them has changed. For this reason, LIGO is based on the design of a Michelson interferometer, as seen in Figure 1.2. This device uses the light from a laser, splits it using a half-silvered mirror (meaning that the mirror is half reflective and half transparent), directs the light down the arms of the device, bounces it off two mirrors and finally directs the light back down the arms, where they recombine at the beamsplitter. The combined beam is observed by a photodetector. If there is no change to the length of the arms, the light recombines deconstructively and no light is seen at the output of the detector. If the length of the arms change, the light will not completely deconstruct, and the sensor at the output will detect light.

This is, of course, an extremely simple and idealized version of the actual detector. Gravitational waves from astrophysical sources have an extremely small amplitude by the time they reach earth. The effect of the gravitational wave is measured in strain h, which is the change of length over length: $h = \frac{\delta L}{L}$.
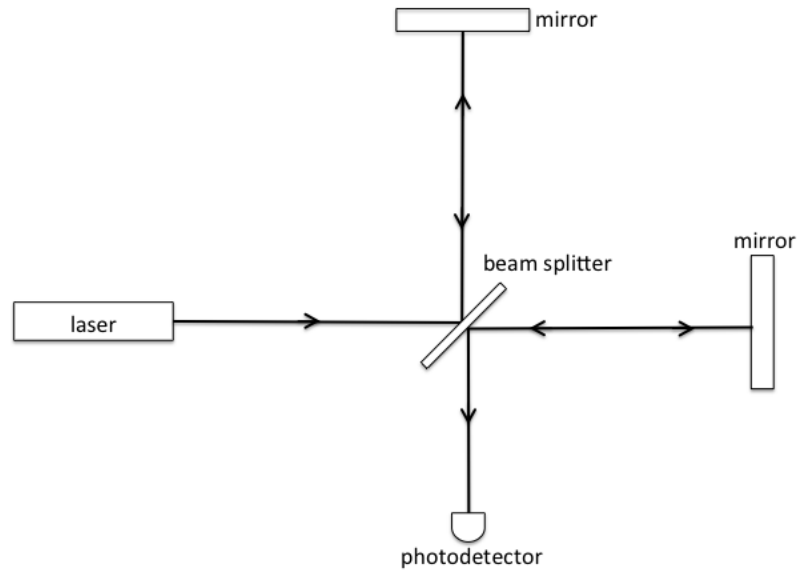
Figure 1.2: A Michelson-type interferometer - a simplified layout of a GW interferometer. Image is from [19].

In other words, as a gravitational wave travels through space, it stretches space proportionally to the length of space being measured over. In order to detect gravitational waves, the length of the interferometer arms need to be as long as feasibly possible, so as to maximize the detectable effect on the change in length of space. The arms of the detector are therefore four kilometers in length. In addition, noise in the detector must be minimized so that the gravitational-wave signal stands out as much as possible from the background noise.

1.3   It's too loud in here

There are many different types of fundamental noises inherent to the detector, the most significant of which can be seen in Figure 1.3. The biggest contributors are seismic noise, low-frequency rumblings from the earth; thermal noise, mid-range noise from the vibrations of particles in the detector itself; and photon shot noise, high-frequency noise caused by inconsistencies in the arrival time of photon packets in the laser beam, as well as many other noise sources. Each of these noise types have unique solutions to mitigate the noise as much as possible. Seismic noise is damped using quadruple pendulums on top of isolated platforms. Photon shot noise is controlled using extremely high-powered lasers. Scattering of light off of particles in the air is dealt with by creating the world's second largest vacuum system. These are just a few examples of
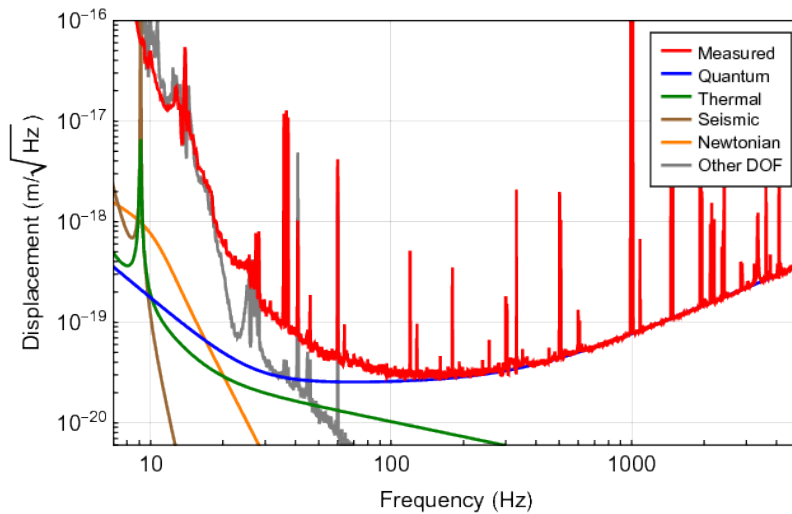
Figure 1.3: This plot shows the noise curve for Advanced LIGO. The x-axis is the frequency range in which LIGO is most sensitive. The y-axis is the displacement of the mirrors, which can be interpreted as displacement at different frequencies caused by noise. The red line indicates the measured noise curve, while the smooth solid lines represent different known sources of noise; blue for quantum shot noise, green for thermal noise, brown for seismic noise, and orange for Newtonian gravitational noise caused by surface ground motion. "Other DOF" refers to measured noise correlated to the auto-alignment system and auxillary length channels. (This figure is from Ref. [20].)

the many efforts put in to create the most effective gravitational-wave detector possible [21]. Similarly, Virgo has undergone many upgrades to become Advanced Virgo [22].

Even with all these efforts in place, there are still instances of noise transients in the detector. These can occur for a variety of reasons, from airplanes creating Doppler-shifting transients to thirsty ravens scraping at built-up ice on pipes [23]. Detector characterization is used to identify these noises sources and either mitigate this noise at the source (where possible) or to remove the noise from the gravitational-wave strain data. For the example of ravens pecking at pipes, the pipes were insulated to prevent the ice build-up from being exposed. In other cases, the noise transients need to be removed directly from the detector data itself. This can be done by using a windowing function to zero out loud noise transients, as can be seen in Figure 1.4. In extreme cases, data with extreme levels of noise must be removed from anaylses entirely. These advances in detector technology and noise suppression has allowed us to detect numerous gravitational waves.
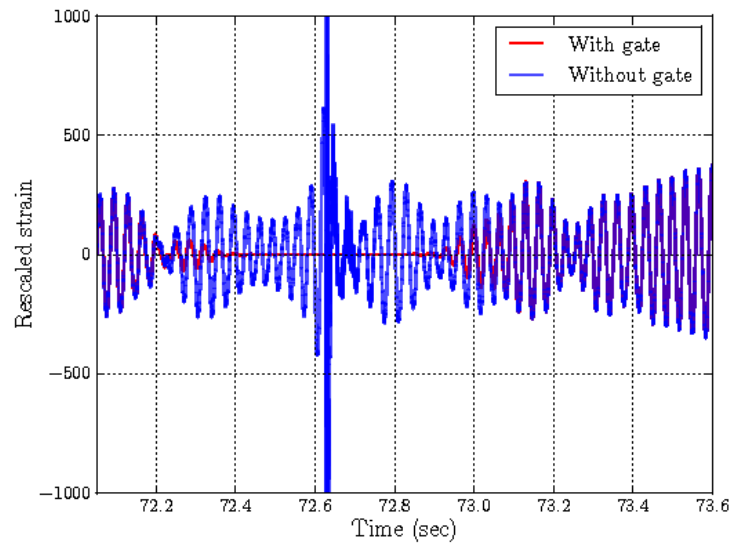
Figure 1.4: This plot shows the effect of a Tukey windowing function on a noise transient in the data. The x-axis represents time (starting from the beginning of the chunk of data). The y-axis represents the whitened strain data (with the very low and very high seismic noises damped, as is used in the offline gravitational-wave search, PyCBC). The blue line represents the data with no windowing, thus including the large noise transient at around 72.6 seconds. The red line shows the effect the Tukey window has on the data, effectively zeroing out the noise transient so it does not affect the search. (The effects of this Tukey window on the search for gravitational waves from binary systems is explained in more detailed in the paper where this plot is from, Ref. [24].)

1.3.1 The First Detections

On September 14th, 2015, LIGO detected the gravitational wave GW150914 [3]. This was a landmark event, being the first gravitational-wave to ever be directly detected. The source of this gravitational wave was a binary black hole system approximately 410 Mpc away. The black holes had masses of about 29 and 36 solar masses, resulting in an approximately 62 solar mass black hole. The black holes radiated about 3 solar masses of energy away as gravitational waves during its merger, meaning binary black hole mergers are some of the most energetic events in the universe. In the same analysis period O1 (called an *observing run*), another binary black hole event was detected, GW151226 [4], which had significantly smaller black holes in its source binary.

More black hole binaries were found in the following observing run, O2: GW170104, GW170608 and GW170814 [5, 6, 8]. These brought more information about black holes and their populations, but we hoped for a new source that would shed a little light on an exotic celestial body. GW170814

was also the first gravitational wave detected in conjunction with Advanced Virgo, allowing for the best sky localization up to that point. At the end of the run, we detected GW170817, the first gravitational wave from a binary neutron star system. This was found simultaneously in gravitational waves [8] and across the electromagnetic spectrum, including as a gamma ray burst named GRB170817a [9]. Over the following few weeks, the electromagnetic component went through a variety of wavelengths, being seen as an optical kilonova [25] and an X-ray afterglow [26]. These led to lots of new information about our universe, including contstraining the nuclear equation of state [12] and observations of the kilonova matched predictions for the optical imprint from radioactive decay of r-process nuclei [27].

Much can be learned from these gravitational-wave signals. However, much of what we can learn about the universe rests on what information we can extract about the source binaries from the gravitational wave signals. In my research, I describe a novel way for rapidly estimating the source parameters for a gravitational wave and a limitation on our ability to learn about a binary system's distance and inclination.

1.4   My Research

This details the contributions I have made over the past two years to the field of gravitational-wave astronomy. These range from a new method of rapidly identifying parameters of the source of a gravitational wave from a binary system to testing our ability to measure the inclination of such a binary.

1.4.1   Rapid Parameter Estimation

Since the era of gravitational-wave astronomy has just begun, we have much to learn from these exotic phenomena. One method of learning more from new detections is by identifying their electromagnetic counterparts. GW170817 marks the first of these multimessenger events, which was identified as a gravitational wave from binary neutron stars and was then coincidentally identified across the electromagnetic spectrum, in the form of gamma rays, optical light, infrared radiation and X-rays [9, 25, 26, 28, 29]. Quickly estimating the parameters of this type of gravitational wave would allow our astronomer colleagues to have more information and could aid in the localization and identification of electromagnetic counterparts. For example, the ejecta and EM signature emanating from a binary neutron star varies as a function of mass [27].

Low-latency pipelines have been developed to quickly identify gravitational-wave signals in LIGO and Virgo data [30]. A secondary pipeline can be used to more precisely estimate the parameters of the gravitational wave so that collaborators can more precisely know what to look for and where. Our parameter-estimation pipeline uses an intuitive method of creating a gridded set of gravitational-wave templates and compares them to the data around the time of the detection. This method mimics the topology of the gravitational wave search pipelines, and allows us to use more information from the initial search to focus our parameterization of the binary. By seeing which templates are most similar to the data set, we can approximate which binary parameters the data most supports. We can use the fall off of the templates' similarity over the parameter space to estimate the most likely parameters, their standard deviation and the confidence regions for the signal. Using the phase and timing differences between the signal in each detector, we can also estimate the signal's origin in the sky. Our intuitive match filtering method allows people unfamiliar with the parameter estimation process to better understand how the low-latency search pipelines are generally laid out.

1.4.2   Estimating Inclination

Next, we characterize LIGO's ability to measure the inclination of a binary. The effect of a gravitational wave is weaker when the source is far away from Earth, since the amplitude of the wave is inversely proportional to the distance it has traveled. If the gravitational-wave signal is coming from a binary star system, a binary system whose oriented directly toward or away from us will have a stronger signal than a binary system which is oriented perpendicular to us. This edge-on orientation would prevent us from seeing one of the polarizations of the gravitational wave, meaning we only measure half of the possible amplitude from the gravitational wave. We can therefore see that a degeneracy exists between the distance from the source and the inclination of the binary system.

Being able to measure the distance and inclination accurately could be key for various astrophysical areas of research. Some astrophysicists posit that being able to identify the distance for various signals from binary black hole systems will allow us to constrain the Hubble constant [11]. Others predict that we can expect different electromagnetic radiation at different opening angles for gamma-ray bursts [27].

For this reason, we explore LIGO's ability to measure the inclination of a

binary system. We do this by estimating the change in signal-to-noise ratio over the inclincation-distance parameter space. This allows us to make a probability density plot for various hypothetical signals, allowing us to compare the probability distribution we would expect to see for different signals. We also investigate this for the specific example of the detected signal GW170817 to verify that our method works and aligns with current parameter estimation publications.

Chapter 2

Estimating Inclination

With its ground-breaking detections in the first years of its operation, the upgraded LIGO and Virgo detectors have opened up the door to discovering new information about the universe. The collaboration's many gravitational-wave (GW) detections from binary systems, including GW150914 [3] and GW170817 [8] have allowed us to draw new insights from these astrophysical sources. These developments include constraining the nuclear equation of state [12] and constraining binary black hole populations [31, 32]. With more detections, we hope to learn even more about our universe, such as more accurately measuring the Hubble constant H_0 as suggested in Ref. [33] and [11] or detailing the opening angle for gamma ray bursts ($GRBs$) from binary neutron star systems (BNS) [34, 27, 35]. However, both of these measurements rely on the accurate measurement of the distance to the binaries and the inclination of their orbital angular momentum with respect to the line of sight. A degeneracy exists between distance and inclination making the measurement of these two parameters very difficult. Of the compact binary detections made by LIGO and Virgo, only the BNS merger GW170817 has had a tightly constrained inclination and distance. The detection of a kilonova afterglow allowed for an accurate distance measurement [36, 37], breaking the degeneracy with inclination. When this type of external information is unavailable, the degeneracy severely limits our ability to measure these parameters.

In this chapter, we will show that this degeneracy is typical for binary mergers. The measured amplitude and phase of the gravitational-wave signal encode the properties of the binary. In particular, it is the differing amplitude of the two polarizations of the gravitational waveform that allow us to determine the binary inclination. However, the plus ($+$) and cross ($\times$) polarizations have nearly identical amplitudes at small inclination angles (less than

45°) and significantly lower amplitudes at large inclination angles (greater than 45°). This leads to two simple observations: first, the signal is strongest for binaries which are close to face-on ($\iota \sim 0$) or face-away ($\iota \sim 180°$) and thus we will be observationally biased to detecting binaries whose orbital angular momentum is well-aligned (or anti-aligned) with the line of sight [38, 39]. Second, for small angles, the amplitudes of the two polarizations are close to equal and we cannot measure distance or inclination separately. Therefore, for the majority of detections, this face-on degeneracy will limit our ability to constrain both electromagnetic (EM) emission models and the Hubble constant. There are various ways to break this degeneracy, such as using the EM measured distance or using jet modelling to constrain the opening angle of a GRB. These techniques were used to improve the constraints on the inclination and distance for the BNS merger GW170817 [40, 41, 42, 43, 44].

Since an inclined binary system would produce both a high-amplitude plus polarization and a lower-amplitude cross polarization, creating a network of detectors which is sensitive to both the plus and cross polarization has been suggested to constrain the inclination using only gravitational waves [45]. A single detector is sensitive to just one polarization. Hanford and Livingston are almost aligned, and see essentially the same polarization. While Virgo is anti-aligned and is sensitive to the orthogonal polarization. The addition of Kagra [46] and India [47] would further increase the network's sensitivity to the orthogonal polarization. Thus it is hoped this network could better constrain the inclination angle and distance. We examine this possibility of constraining the inclination using only the measurement of the two GW polarizations.

There have been many studies looking at inclination constraints. From the GRB perspective they are largely divided into two groups: the first focuses on exploring the possibility of nailing down the viewing angle by comparing the rate of GRB sources observed in GWs with those in gamma rays [48, 34, 49]. The second focuses on measurements for individual detections, mainly in the case where the event has been three dimensionally localized by an EM counterpart [50, 51, 52] Inclination constraints have also been discussed in the context of distance estimates for cosmology [53, 38, 54] and as part of wider parameter estimation investigations [55, 56]. It was noted in Ref. [38] that adding detectors to a network did not seem to greatly improve the inclination measurement. Here we push this to this extreme by including all current and proposed future ground-based observatories. In particular, we investigate a network that would measure both polarizations equally as would be expected

over the majority of the sky for the Einstein Telescope (*ET*) [57].

2.1 Measuring Distance and Inclination

When a gravitational-wave signal is observed in the data from the LIGO and Virgo instruments, the goal is to obtain estimates for the parameters that describe the waveform. Typically, Bayesian inference [58, 59, 60] is used to obtain a posterior distribution for the parameters of the system $\boldsymbol{\theta}$ given the observed data $\mathbf{d}$. As described in detail in Ref. [61], the likelihood of obtaining data $\mathbf{d}$ given the presence of a signal $h(\theta)$, and under the assumption of Gaussian noise characterized by a power spectrum $S(f)$, is

$$\Lambda(\mathbf{d}|\boldsymbol{\theta}) \propto \exp\left[-\frac{1}{2}\left(\mathbf{d}-h(\boldsymbol{\theta})|\mathbf{d}-h(\boldsymbol{\theta})\right)\right]. \tag{2.1}$$

Here, we have introduced the weighted inner product

$$(a|b) := 4\mathrm{Re}\int_0^{f_{\max}} \frac{\tilde{a}(f)\tilde{b}(f)^\star}{S(f)}\,\mathrm{d}f. \tag{2.2}$$

The likelihood for a network of detectors is simply the product of likelihoods for the individual detectors:

$$\Lambda(\mathbf{d}|\boldsymbol{\theta}) \propto \exp\left[-\frac{1}{2}\sum_{i\in\mathrm{dets}}\left(\mathbf{d}_i-h_i(\boldsymbol{\theta})|\mathbf{d}_i-h_i(\boldsymbol{\theta})\right)\right]. \tag{2.3}$$

The posterior distribution for parameters $\boldsymbol{\theta}$ given the data $\mathbf{d}$ is given as

$$p(\boldsymbol{\theta}|\mathbf{d}) \propto \Lambda(\mathbf{d}|\boldsymbol{\theta})p(\boldsymbol{\theta}), \tag{2.4}$$

where $p(\boldsymbol{\theta})$ is the prior distribution for the parameters. The posterior distributions are typically calculated by performing a stochastic sampling of the distribution [59, 60, 62, 63, 64]. Distributions for a subset of parameters are obtained by marginalizing, or integrating out, the additional parameters.

In this analysis, we are interested in obtaining the joint distribution of the luminosity distance d_L and binary inclination ι. This is calculated as

$$p(d_L, \cos\iota|\mathbf{d}) = \int d\boldsymbol{\mu}\,\Lambda(\mathbf{d}|\boldsymbol{\mu}, d_L, \cos\iota)p(\boldsymbol{\mu}, d_L, \iota) \tag{2.5}$$

Typically, $\boldsymbol{\mu}$ contains all parameters describing the system, including the

masses, spins, sky location, orientation and parameters describing the nuclear equation of state. For our work, we consider a simplified model, for which the only additional parameters $\boldsymbol{\mu}$ are the binary's polarization ψ and coalescence phase ϕ_o. We choose uniform priors on these parameters, as well as a uniform prior on $\cos \iota$, which leads to a uniform distribution of binary orientation. Furthermore, we use a uniform-in-volume prior for the distance $p(d_L) \propto d_L^2$. For binaries at greater distance, we need to take into account cosmological effects and use a prior with sources uniform in comoving volume and merging at a constant local rate. At even greater distances, the local merger rate would follow the star formation rate [65], which peaks at $z \sim 2$. We take this into account later in this chapter for binary black hole systems, (BBH), detected at far distances using future detector networks.

In our approximation, we fix the sky location and arrival time of the signal, as well as the masses and spins of the system. Fixing the sky location is reasonable, as one of the main motivations for this work is to investigate the accuracy of gravitational-wave measurements of distance and inclination after the signal has already been identified and localized by the detector network. We also investigate how inclination measurements from gravitational-wave observations can be combined with electromagnetic observations. An unknown sky location will only lead to larger uncertainties in the distance and inclination measurements arising from varying detector sensitivities over the sky.

While the masses and spins of the binary will not be known, in most cases these parameters have little impact on the inferred distance and inclination. Binary neutron star systems are in-band in ground-based detectors for a large number of cycles, $\mathcal{O}(10^5 - 10^6)$, allowing the accurate measurement of the phase evolution of the binary. Hence the chirp mass $\mathcal{M}$ — the parameter determining the leading order phase evolution — is measured with great precision. For BNS, the GW amplitude scales as $\mathcal{M}^{\frac{5}{6}}$, so uncertainty in mass has no effect on the distance d_L. In the analysis presented here, we focus only on the dominant gravitational-wave emission at twice the orbital frequency. For unequal-mass systems, the other gravitational-wave harmonics can significantly affect the waveform, particularly when the binary has a high mass ratio, i.e. one of the compact objects is significantly more massive than the other [66]. This can lead to improvements in the measurement of the binary orientation [67].

Spins which are misaligned with the orbital angular momentum lead to precession of the binary orbit [68] which can, in principle, lead to an improved measurement of the binary orientation. To date, there is no evidence for pre-
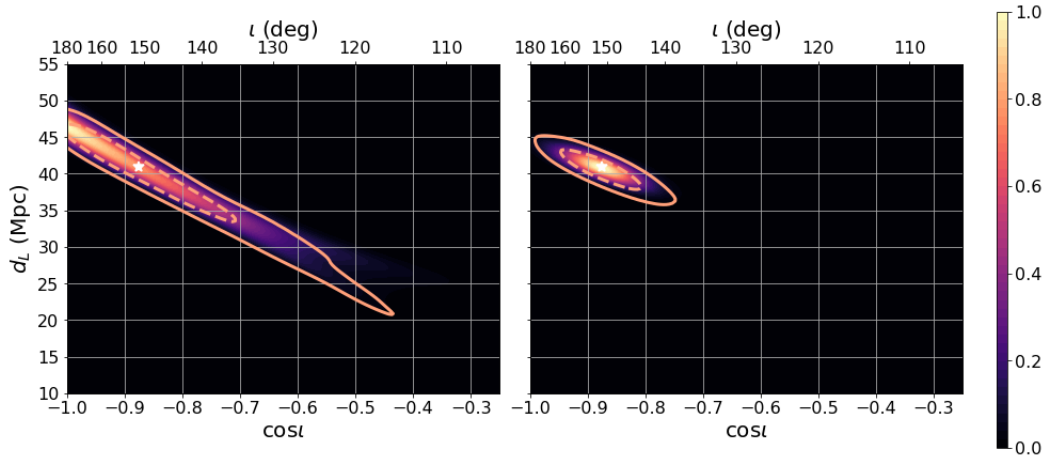
Figure 2.1: The marginalized posterior distribution for the distance and inclination of the binary neutron star system GW170817, detected with an alignment factor $\alpha \sim 0.13$ and signal to noise ratio $\rho \sim 32$. The alignment factor α refers to the relative sensitivity to the cross polarization when a frame of reference is chosen to maximize the sensitivity to the plus polarization in the detector frame, $F_\times = \alpha F_+$. The left plot was generated using only the data from gravitational-wave detectors, while the right plot also uses the independent distance measurement (40.7 Mpc, ± 2.4 Mpc at 90% confidence) from electromagnetic observations. The coloured portion of the plot shows the probability distribution obtained using our approximate analysis, normalized such that the peak probability is 1. The orange contours represent the 90% and the 50% confidence intervals obtained by performing the full analysis of the LIGO-Virgo data (posterior samples are publicly available here: https://dcc.ligo.org/LIGO-P1800061/public) [43].

cession in the observed GW signals [69, 70, 71, 72, 73], so the approximations discussed here would therefore be applicable. Furthermore, neutron stars are not expected to achieve a spin high enough to have observable precession.

To verify that fixing the masses and spins has limited impact on the recovered distance and inclination, we compare results from our model with those from the full parameter estimation of GW170817. We recreate the posterior distribution for the multi-messenger signal GW170817, with and without distance information from the coincident electromagnetic signal, and compare it to the full, Bayesian parameter estimation, with a fixed sky location, using the observed LIGO and Virgo data [43]. The results are shown in Figure 2.1. To generate our results, we approximate the data **d** by a gravitational-wave signal at a distance of $d_L = 40.7$ Mpc [40] and an inclination of 153° [43]. We then generate a posterior distribution for the four dimensional parameter space of distance d_L, inclination ι, polarization ψ and coalescence phase ϕ_0. From this we calculate the posterior distribution, $p(d_L, \iota | \mathbf{d})$ by marginalizing

over the polarization and phase angles. As is clear from the figure, our approximate method gives a posterior on distance and inclination which is in excellent agreement with the full results from the real data.[1]

The results in Figure 2.1 show an example of the degeneracy in the measured values of the distance and binary inclination. The 50% confidence interval includes both a face-away binary at a distance of 45 Mpc and a binary inclined at 135° at a distance of 35 Mpc. It is only when the gravitational-wave data is combined with the electromagnetically determined distance 45 ± 2.4 Mpc [40] that the binary inclination can be accurately inferred. The degeneracy between distance and inclination arises directly from the dependence on the gravitational waveform on these parameters, and has been discussed several times previously [53, 55, 38].

To understand why distance and inclination are degenerate, we must look to the waveform of gravitational waves emitted from a binary system. The gravitational-wave signal, $h(t)$, incident on a gravitational-wave detector is given by [74]:

$$h(t) = F_+(\alpha, \delta, \chi) h_+(t) + F_\times(\alpha, \delta, \chi) h_\times(t), \qquad (2.6)$$

where F_+ and $F_\times$ are the detector response to the plus and cross polarizations, respectively. The detector responses depend on the location (α, δ) of the source. In addition, we must specify a polarization angle χ to fully specify the *radiation frame.* It is common [75, 76] to define a dominant polarization frame, for which the detector network is maximally sensitive to the plus polarization. With this choice, we can naturally characterize the network by its overall sensitivity and the relative sensitivity to the second polarization [75, 77]. This simplifies the comparison of different networks.

For a waveform where it is appropriate to neglect higher order modes and precession, the two polarizations given in Equation 2.6 can be expressed in terms of the two orthogonal phases of the waveform:

$$h_+(t) = \mathcal{A}^1 h_0(t) + \mathcal{A}^3 h_{\frac{\pi}{2}}(t) \qquad (2.7)$$

$$h_\times(t) = \mathcal{A}^2 h_0(t) + \mathcal{A}^4 h_{\frac{\pi}{2}}(t) \qquad (2.8)$$

---

[1]We note that the results in [43] show this distribution as a function of inclination ι instead of $\cos \iota$. This leads to a different distribution, and different 90% confidence intervals as these are defined to be the minimum range that contains 90% of the probability, and this is dependent upon variable choice. As we discuss later, there is no evidence in the GW data alone that the signal is not face-on, and since the prior is flat in $\cos \iota$ we believe that plotting the distribution against $\cos \iota$ leads to a clearer understanding of the distribution.

where $\widetilde{h}_{\frac{\pi}{2}}(f) = i\widetilde{h}_0(f)$. The $\mathcal{A}^i$ are overall amplitude parameters, and depend on the distance D, inclination ι, polarization ψ and coalescence phase ϕ_0 [78, 79]:

$$\mathcal{A}^1 = \mathcal{A}_+ \cos 2\phi_0 \cos 2\psi - \mathcal{A}_\times \sin 2\phi_0 \sin 2\psi \tag{2.9}$$

$$\mathcal{A}^2 = \mathcal{A}_+ \cos 2\phi_0 \sin 2\psi + \mathcal{A}_\times \sin 2\phi_0 \cos 2\psi \tag{2.10}$$

$$\mathcal{A}^3 = -\mathcal{A}_+ \sin 2\phi_0 \cos 2\psi - \mathcal{A}_\times \cos 2\phi_0 \sin 2\psi \tag{2.11}$$

$$\mathcal{A}^4 = -\mathcal{A}_+ \sin 2\phi_0 \sin 2\psi + \mathcal{A}_\times \cos 2\phi_0 \cos 2\psi, \tag{2.12}$$

where $\mathcal{A}_+$ and $\mathcal{A}_\times$ are amplitudes for the plus and cross polarizations in the *source frame*, which is aligned with the binary's orbital angular momentum. They are given by:

$$\mathcal{A}_+ = \frac{d_0}{d_L} \frac{1 + \cos^2 \iota}{2} \tag{2.13}$$

$$\mathcal{A}_\times = \frac{d_0}{d_L} \cos \iota, \tag{2.14}$$

where d_L is the luminosity distance and d_0 is the reference luminosity distance. The variation of the two polarization amplitudes with inclination ι is shown in Figure 2.2. We note that there is an arbitrary choice of the *radiation frame* and this will affect the value of the angles ψ and χ and consequently the values of the $\mathcal{A}^i$. However, the signal observed at the detectors is independent of this choice.

In principle, we should be able to measure all four of the amplitude parameters by accurately measuring both the amplitude and phase of both the plus and cross polarizations of a gravitational wave. From here, we could then infer the distance and orientation of the source binary. However, degeneracies in parameters limits our ability to accurately measure these parameters.

In order to identify the inclination of the binary system using the polarizations of the gravitational wave, we must distinguish the contributions of the plus and cross polarizations. When the binary system is near face-on or face-away, the two amplitudes $\mathcal{A}_+$ and $\mathcal{A}_\times$ have nearly identical contributions to the overall gravitational-wave amplitude. In Figure 2.2, we see the relative difference between plus and cross is less than 1% for inclinations less than 30° (or greater than 150°) and 5% for inclinations less than 45° (or greater than 135°). This is the main factor that leads to the strong degeneracy in the measurement of the distance and inclination.

As we have already described, gravitational-wave detectors with limited

sensitivity will preferentially observe signals which are close to face-on or face-off. In addition, when the binary is close to face-on and the emission is circularly polarized, the waveform is described by a single overall amplitude and phase (as the two polarizations are equal, up to a phase difference of $\pm 90°$). Thus it is no longer possible to measure both the polarization ψ and phase at coalescence ϕ_0 of the binary, but only the combination $\phi_0 \pm \psi$ (with the $+/-$ for face-on/away binaries respectively). This degeneracy, combined with the distance prior, leads to a significantly larger volume of parameter-space which is consistent with face-on, rather than edge-on systems.

To exclude face-on binaries from a marginalized posterior probability distribution on the inclination, the network must accurately measure the amplitude and phase of both of the polarizations. In general, gravitational-wave detectors are not equally sensitive to the two polarizations. For a given sky location, we can define the plus polarization as the linear combination we are most sensitive to and then calculate the relative sensitivity of $\times$. We can think of this as a detector network comprised of a long plus-detector and a shorter cross-detector (a factor of α shorter). Thus we can estimate the proportional sensitivity to the second polarization, called the network alignment factor [75], through the relation $F_\times = \alpha F_+$, where α varies between 0 and 1. Therefore the sensitivity of the network to the second polarization can be determined by looking at the values of α over the sky.

Figure 2.3 shows the distribution of alphas for various detector networks. As might be expected, the sensitivity to the second polarization increases as more detectors are added to the network. For the two LIGO detectors, the typical value is $\alpha \sim 0.1$ because the two detectors have very similar orientations. When the Virgo detector is added to the network, the mode is $\alpha \sim 0.3$ and this increases to $\alpha \sim 0.5$ when KAGRA and LIGO India join the network. The Einstein telescope is a proposed future detector with a triangular configuration [57]. For an overhead source, ET is equally sensitive to both polarizations, giving $\alpha = 1$. While ET does not have equal sensitivity to both polarizations over the whole sky, the majority of signals will be observed with $\alpha > 0.9$. For the future networks, we consider an ET detector complemented by either the advanced LIGO detectors with sensitivity improved by around a factor of three (LIGO Voyager), or by one or two Cosmic Explorer detectors [80, 77]. When the ET detector dominates the network's sensitivity, we have excellent measurement of both polarizations but, in the CE-ET networks where CE is more sensitive, the sensitivity to the second polarization is comparable to the

current networks.

2.2 Accuracy of measuring distance and inclination

Now that we understand how the degeneracy between inclination and distance arises, we can explore the expected accuracy with which these parameters will be measured in various gravitational-wave detector networks. For concreteness, in the examples that follow, we fix the SNR of the signals to be 12. While this might seem low, we note that for a detection threshold of 8, the *mean* SNR observed from a uniform-in-volume population would be 12 [39]. We discuss higher SNR signals later in the chapter. Rather than specifying a network and sky location, we instead investigate the ability to measure distance and inclination as we vary the network's relative sensitivity to the second polarization, encoded in the variable α. For convenience, we fix the masses of the system to be $1.4 M_\odot$ and set the sensitivity of detector network to the plus polarization of GW to be equal to that of a single advanced LIGO detector at design sensitivity for an overhead source. This places a face-on system at approximately 300 Mpc at SNR of 12. For inclined systems, the distance will be smaller to ensure that the network still receives an SNR of 12. While we have fixed the masses and detector sensitivities to make the plots, the results are essentially independent of these choices, up to an overall rescaling of the distance. Thus the results will be applicable to any system for which it is reasonable to neglect precession effects and the impact of higher modes in the gravitational waveform.

Let us begin by considering a network with relatively poor sensitivity to the second GW polarization, with $F_\times = 0.1 F_+$. This is typical for the LIGO Hanford-Livingston network, and is common for the LIGO-Virgo network, as described in Figure 2.3 We consider two signals, both with SNR of 12, but one which is face-on ($\iota = 0$) at a distance of 300Mpc while the second is edge-on ($\iota = 90°$) at a distance of 150 Mpc and a polarization angle of $\psi = 0$ so that the GW power is contained in the plus polarization. The first column of figures in Figure 2.4 shows the likelihood, maximized over ϕ_0 and ψ, across the distance-inclination plane. Note that the contours here are calculated for our simplified model and do not represent the results of full parameter estimation analyses, as they did in Figure 2.1. As expected, the maximum likelihood occurs at values of distance and inclination which exactly match the

signal. We observe a degeneracy in distance and inclination, so that there is some support for the edge-on binary to be face-on (or face-away). There is also degeneracy for the face-on binary, which is marginally consistent with an edge-on binary, but face-away orientation can be excluded. With an SNR of 12 and $\alpha = 0.1$, for a face-on signal we expect an SNR of about 1.2 in the cross polarization. These results show that the presence or absence of this signal is sufficient to down-weight, but not exclude, an edge-on orientation when the source is really face-on, and vice-versa. For a face-away system, the expected signal in the cross polarization is the same amplitude, but entirely out of phase from the face-on system, and this is sufficient to distinguish the two.

In the second column, we show the likelihood, marginalized over the polarization and phase angles. This marginalization does not have a significant impact on the face-on binary, but completely changes the distribution for the edge-on binary — with the marginal likelihood now peaked at $\cos \iota = \pm 1$. Typically, we would expect to be able to measure the two phase angles with accuracy $\sim 1/\rho$ thus to a crude approximation, marginalizing over the phase angles would give a contribution $\approx (1/\rho^2)\Lambda_{\max}$, where $\Lambda_{\max}$ is the maximum likelihood. When the binary is recovered (nearly) face-on the two amplitudes $\mathcal{A}_{+,\times}$ are (nearly) equal. Consequently, the signal is circularly polarized, with the phase determined by $\phi_0 + \psi$. Changing the value of $\phi_0 - \psi$ has no effect on the waveform. Thus, when marginalizing over the polarization and phase, we obtain a factor $\sim (\pi/\rho)\Lambda_{\max}$. Thus, for this signal at SNR 12, marginalizing of the polarization and phase will lead to a relative increase of nearly 40 in favour of the face-on signal.

Finally, in the third column, we include the distance prior by re-weighting by d_L^2 to place sources uniformly in volume. This gives an additional factor of four weighting in favour of the face-on signal over the edge-on one. Once all these weightings are taken into account, the probability distributions between a face-on and edge-on signal are similar for a network with this sensitivity. The edge-on signal has slightly more support at $\cos \iota \approx 0$, and this is still included at 90% confidence. Additionally, the edge-on signal is consistent with either a face-on or face-away orientation. It may seem strange that we will not recover the parameters of the edge-on system accurately. However, this is appropriate. As we have discussed, the volume of parameter space consistent with a face-on system is significantly larger than for the edge-on case. Thus, even if we observe a signal that is entirely consistent with an edge-on system, it is more likely that this is due to a face-on system and noise fluctuations leading to the

observed signal than it is that the signal is coming from an edge-on system.

Our next example investigates differing inclinations for a signal detected by a network with an $F_\times = 0.5F_+$, a network with half the sensitivity to the cross polarization as the plus polarization. This is the predicted mean sensitivity expected for the best near-future detector network consisting of the Hanford, Livingston, Virgo, KAGRA and LIGO-India detectors. Again, the SNR is set to 12 for all hypothetical signals, and now we consider three different inclinations: $\iota = 0$ (face-on) and two inclined signals, one with $\iota = 66°$ and the other with $\iota = 78°$. In Figure 2.5, we show the posterior distribution for distance and inclination for the three cases. Here, we have marginalized over the phase angles and included the distance prior weighting, so the plots are equivalent to the third column of plots in Figure 2.4.

The leftmost plot shows the probability distribution for a face-on signal. This distribution is similar to the one for $\alpha = 0.1$, though now the most inclined and face-away points in parameter space are excluded from the 90% credible region. The second plot is for a binary inclined at $66°$ ($\cos \iota = 0.4$). Here, the peak of the inclination distribution corresponds to a face-on system and, indeed, the posterior is nearly identical to that obtained for the face-on system. Thus, for a typical system with close-to-threshold SNR we will remain unable to distinguish between face-on signals and those inclined at $60°$ based on gravitational-wave observations alone. The best near-future detector therefore would be unable to measure a difference in inclination between these two hypothetical signals. Only once the inclination reaches $78°$ ($\cos \iota = 0.2$) does the distribution peak at an inclined signal, as in the rightmost plot. However even for inclinations as great as this, the 90% credible region cannot exclude face-on and extends across all orientations from face-on to edge-on. In this case it is not possible to clearly distinguish the binary orientation. For values of $\cos \iota < 0.1$ the posterior is peaked at the correct value of ι and excludes face-on from the 90% credible region.

The results shown in Figures 2.4 and 2.5 show the general features of the distance and inclination distribution. It is characterized by three components: one consistent with a face-on signal, one with an face-off signal and a third contribution peaked around the true values of distance and inclination. In all of the cases we have shown, only one or two of the contributions are significant. There are, however, cases where we obtain three distinct peaks in the posterior for the inclination, although these are rare. In Appendix B of [81], an approximate expression for probability associated with each peak was obtained, which

Network	$0° \leq \iota < 45°$			$45° \leq \iota < 60°$		
	face on	mixed	edge on	face on	mixed	edge on
HL	100%	0%	0%	97%	3%	0%
HLV	100%	0%	0%	86%	13%	1%
HLVK	100%	0%	0%	78%	21%	1%
HLVKI	100%	0%	0%	67%	32%	1%
Network	$60° \leq \iota < 75°$			$75° \leq \iota < 90°$		
	face on	mixed	edge on	face on	mixed	edge on
HL	80%	18%	2%	47%	32%	21%
HLV	47%	44%	9%	29%	27%	44%
HLVK	27%	59%	14%	17%	20%	63%
HLVKI	7%	72%	21%	7%	13%	80%

Table 2.1: The table shows the ability of various networks to distinguish the orientation of a population of binary mergers with given inclination, ι. For each network and range of ι, we give the percentage of binaries for which the posterior on the inclination peaks at $\iota = 0$ or $180°$ (face-on) and this peak contains over 90% of the probability; those binaries for which the recovered inclination peaks at the correct value, and greater than 90% of the probability is consistent with this peak (inclined); and those for which the posterior includes significant contributions for both face-on and inclined orientations (uncertain). For all networks, essentially all binaries with $\iota < 45°$ will be recovered face-on. As the inclination increases further, the ability to clearly identify the binary as inclined increases significantly with the number of detectors in the network as this improves the average sensitivity to the second gravitational-wave polarization.

is valid for networks sensitive to a range where a d_L^2 prior is still appropriate. This provides an analytic expression for the probability associated to each of the three contributions, as a function of SNR, inclination, polarization and the network sensitivity to the second polarization, encoded in the variable α.

To get a sense of how accurately binary inclination will be measured, we simulated a set of $1,000,000$ events uniformly in volume and determined those which would be observed above the detection threshold of the network (typically leaving 30,000-80,000 events). For each event, we then determine whether the event would be recovered as definitely face-on — over 90% of the probability associated to the face-on (and face-away) components of the distribution — definitely inclined or uncertain. These results are summarized in Table 2.1, for a series of networks each with an increasing number of detectors. For all networks, essentially all events with a true inclination less than $45°$ will be recovered face-on. Only for those events with inclination greater than $45°$ do we start to be able to distinguish the orientation. Between 45 and $60°$,

networks with three or more detectors will classify a small fraction of events as inclined, and this fraction increases with both the inclination of the system and the number of detectors (which directly effects the typical value of α). However, even for events which have an inclination greater than 75°, the LIGO Hanford–Livingston network would recover half as face-on and only 20% as definitely not. This improves for the five detector network where less than 10% are face-on, and 80% are clearly identified as being inclined.

Next, let us consider the general accuracy with which we can measure the inclination for a binary which is (nearly) face-on. In this case, the distribution for the inclination angle can be approximated in a simple way. If we begin by assuming that the degeneracy between distance and inclination is exact, then orientations with $|\cos\iota| \approx 1$ are preferred due to the prior on the distance. This can be clearly seen by comparing the second and third columns of plots in Figure 2.4. The distribution in the second column (when we don't apply the uniform-in-distance weighting) shows a broad degeneracy with equal probability along lines of constant $\mathcal{A} = \cos\iota/d_L$. It is only by applying the distance re-weighting that the peak shifts more to $\cos\iota = 1$. For a fixed value of ι, we wish to integrate over a given distribution, $p(\cos\iota/d_L)$. Thus we obtain

$$
\begin{aligned}
p(\cos\iota) &= \int d_L^2 p(\cos\iota/d_L)\mathrm{d}d_L \\
&= \int \cos^3\iota\, \mathcal{A}^{-4} p(\mathcal{A})\mathrm{d}\mathcal{A} \\
&\propto \cos^3\iota
\end{aligned}
\tag{2.15}
$$

Thus, it follows that, where the degeneracy holds, the posterior on $\cos\iota$ will be proportional to $\cos^3\iota$. In Figure 2.6, we show the posterior for three examples of face-on signals : SNR $\rho = 12$ with $\alpha = 0.1$ and 0.5, and SNR $\rho = 50$ with $\alpha = 1$. All three distributions follow the $\cos^3\iota$ distribution for small inclinations. The high-SNR signal deviates at around 30° — at this inclination there is enough difference from a circularly polarized signal for larger inclinations to be disfavoured. However, for the lower-SNR signals (and also lower values of α) the approximation remains accurate to greater than 45°.

We can improve the approximation by noting [81] that the SNR lost by projecting an inclined signal onto a circular signal is

$$
\Delta\rho^2 = \frac{\alpha^2\rho^2}{(1+\alpha^2)^2}\frac{(1-\cos\iota)^4}{4}\,.
\tag{2.16}
$$

This loss in SNR leads to a reduction in the likelihood associated with the inclined signal, which causes the probability distribution to fall off more rapidly away from $\iota = 1$. In particular we obtain:

$$p(\cos \iota) \quad \propto \quad \cos^3 \iota \exp\left(-\frac{\Delta\rho^2}{2}\right). \qquad (2.17)$$

We can use this expression to determine how well a network with sensitivity α would be able to constrain a signal's inclination ι, given the SNR of the signal. In Figure 2.7, we specifically look at how tightly we can constrain a face-on signal. We can see that for low-SNR signals or for networks with little sensitivity to the cross polarization, GW observations will only be able to constrain the signal to being less than about 45°. Even with an extremely loud signal and a very sensitive detector network, we are only able to constrain the signal to about 30°. It's important to note here that at these SNRs, higher order modes or precession in the gravitational-wave signal may be observable. If these are detected, the degeneracy between distance and inclination would be broken, and we would be able to more tightly constrain the inclination.

Finally, it is interesting to consider what effect the inclination distance degeneracy would have on the mass estimate of binary black holes. GW detectors actually measure the redshifted mass $\mathcal{M}_{det} = (1+z)\mathcal{M}_{source}$ where the subscripts denote detector-frame and source-frame respectively [55]. There is no way to determine the redshift directly from the gravitational waveform of a binary black hole. However the measured value of the luminosity distance can give the redshift if a cosmology is assumed. In this way, the inclination distance degeneracy will map to an uncertainty in the rest-frame masses. For the next generation of gravitational-wave detectors, which will be sensitive to BBH mergers throughout the universe, the uncertainty in the redshift will likely be the dominant uncertainty in the masses. As such, we explore the inclination measurement with ET for a BBH merger at a redshift of $z = 10$ with intrinsic masses of a $10M_\odot - 10M_\odot$ corresponding to a detector frame chirp mass of $\mathcal{M}_{det} = 96M_\odot$. We place the source directly above the detector, in the most sensitive part of the sky. In this case, $\alpha = 1$ and $\rho = 20$, where we have assumed standard cosmology [82].

At these cosmological distances, a d_L^2 prior for the distance is no longer appropriate. Rather, we use a distance prior that is uniform in comoving volume where the rest-frame binary merger rate density follows the cosmic star formation rate [65] with a delay between star formation and binary merger Δt,

and a distribution of delay times $p(\Delta t) \propto 1/\Delta t$ [83] (see Section 5 of [77] for details). The new prior peaks at $z \sim 1.4$. Therefore at $z \sim 10$, the nearer, more inclined binaries are *a priori* more likely.

In Figure 2.8 we show the marginalized posterior for three different inclinations: $\iota = 66°$, $\iota = 60°$ and $\iota = 0°$. For the second generation networks in Figure 2.5, the $\iota = 66°$ ($\cos \iota = 0.4$) source is recovered as face-on. With the higher signal to noise ratio and improved sensitivity to the second polarization, ET can identify the signal as edge on. At an inclination of $\iota = 60°$, the degeneracy still extends across $25° < \iota < 70°$, though smaller inclinations are now excluded from the 90% credible interval. This is the effect of the new distance prior which is a factor of 12 larger at redshift 6 than at redshift 10. Thus, though the 90% credible region of the marginalized likelihood extends right up to face-on, the prior is able to partially break the degeneracy. For binaries with inclinations greater than this $\iota > 60°$, the degeneracy extends right up to face-on to a 90% probability interval.

For the face-on binary in the rightmost plot, the prior shifts the peak of the posterior away from the true value. Although the value of the likelihood at face-on and redshift 10 is a factor of 12 larger than it is at an inclination of $60°$ and redshift 6, after the prior re-weighting these two points in the parameter space are equally likely. If the detector frame chirp mass of the binary is measured to be $\mathcal{M}_{det} = 96 M_\odot$, the degeneracy between the inclination and distance results in $\mathcal{M}_{source} = 96 M_\odot$ and $\mathcal{M}_{source} = 61 M_\odot$ being equally likely. The detector-frame chirp mass $\mathcal{M}_{det}$ would be determined to an accuracy similar to the accuracy of the GW phase measurement $\Delta \mathcal{M}_{det}/\mathcal{M}_{det} \sim 1/(\rho \mathcal{N}_{cycles})$ [84, 38]. Parameter estimation for GW150914 yielded a precision in the detector-frame mass estimate of $\Delta \mathcal{M}_{det}/\mathcal{M}_{det} \sim 10\%$ for a comparable SNR [85]. For a larger mass binary, typically fewer cycles of the waveform will be visible in the data. However ET's improved sensitivity at low frequencies compared to LIGO means that we can expect the precision of the detector-frame mass estimate of GW150914 and the ET binary to be roughly the same. Thus the broad uncertainty in the intrinsic masses due to the distance inclination degeneracy $\Delta \mathcal{M}_{source}/\mathcal{M}_{source} \sim 40\%$ will dominate the total error budget.

2.3 Conclusion and Future Work

Our work demonstrates that even with a network equally sensitive to both polarizations of the gravitational wave, we would be unable to precisely measure

the inclination or distance of a nearly face-on binary due to a strong degeneracy between distance and inclination. However, we have focused on non-spinning binaries and assume that the sky location, masses and arrival times of the detectors are all known. Introducing these parameters would increase the uncertainties. Exploring how these parameters affect the overall measurement of the distance and inclination could give a more accurate summary of LIGO's ability to measure distance and inclination.

The degeneracy between inclination and distance described here could be broken in a few different ways: by using distance or inclination from electromagnetic measurements, by detecting higher order modes [67] and by measuring precession [86]. Binary neutron star systems produce a variety of EM signatures, as were observed for GW170817 [8]. Neutron star-black hole binaries (*NSBH*) could produce EM signatures should the neutron star be tidally disrupted. However, tidal disruption only happens at relatively small mass ratios [87]. For larger mass ratios, the neutron star plunges into the black hole creating a deformity which rings down. Interestingly, both precession and higher modes have a larger effect on the gravitational waveform at higher mass ratio [88, 89]. The polarizations of the higher modes have a different dependence on the inclination, and the precession of the orbital plane would result in changing amplitudes for the plus and cross polarizations. These effects can make it easier to identify the inclination angle [67, 89, 86]. For NSBH, the degeneracy can thus be broken by either information from the EM emission or from higher modes or precession. [86] demonstrated that precession would break the distance inclination degeneracy in NSBH for a few binaries with a few values of the precession angle and large, highly spinning black holes. It would be an interesting follow up to this study to explore this with a realistic distribution of spins, to see when precession plays a significant role in measuring binary parameters.
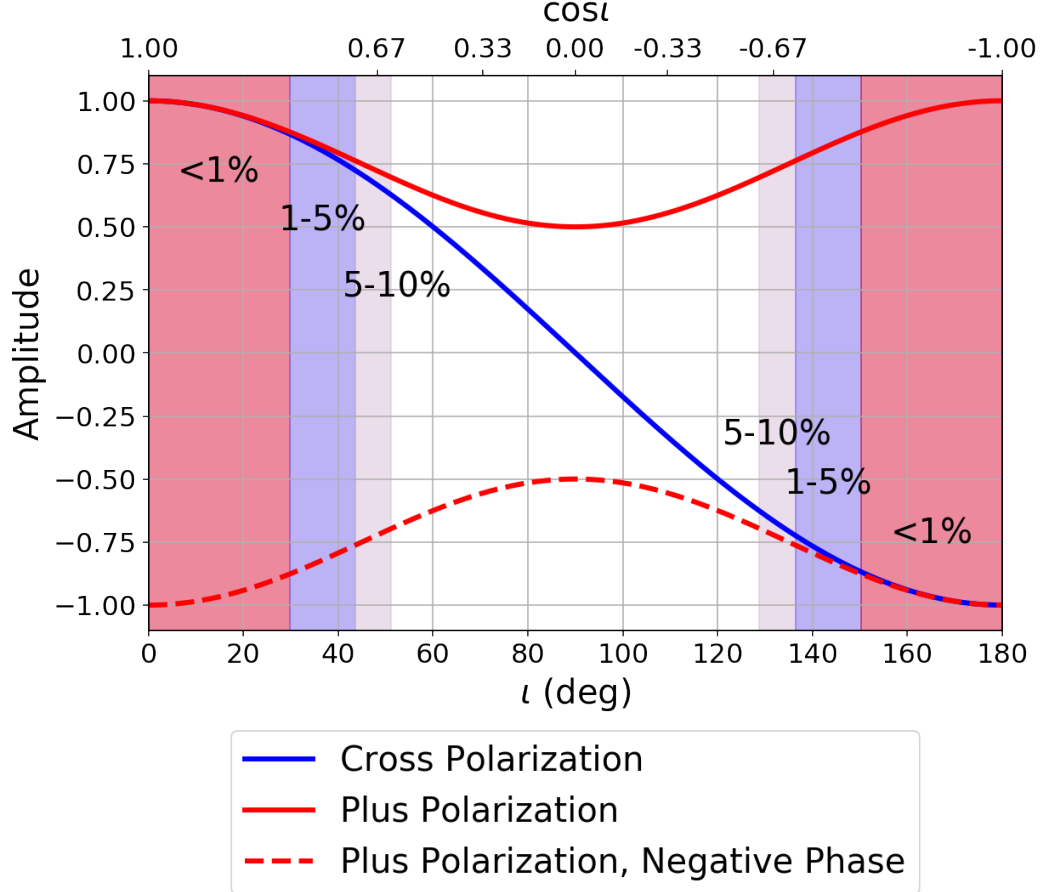
Figure 2.2: The relative contributions of the plus and cross polarizations to a gravitational-wave signal, dependent on the inclination. The red solid line indicates the amplitude of the plus polarization, while the dashed red solid line indicates the amplitude for the plus polarization with a negative phase. The blue solid line indicates the amplitude of the cross polarization. The shaded regions show the percent differences between the plus and cross polarizations. The red portion represents when the plus and cross polarization are less than 1% different. The blue region represents where the polarizations are between 1% and 5% different. The grey region represents where the polarizations are between 5% and 10% different.
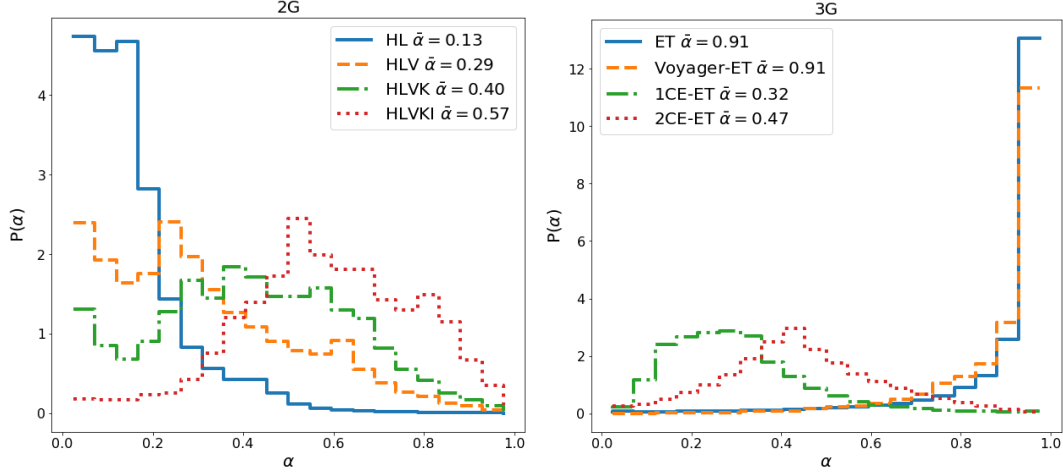
Figure 2.3: The relative sensitivity of detector networks to the second polarization, as encoded in the parameter α, defined through $F_\times = \alpha F_+$ (in the dominant polarization frame where the network is maximally sensitive to the plus polarization). The left plot shows the expected distribution of α for second-generation gravitational-wave networks, while the right plot shows the distribution for potential third generation networks. In both cases, the distribution is the expected distribution for a population of events, distributed uniformly in volume, and observed above threshold in the detector network. Thus, directions of good network sensitivity are more highly weighted. The second generation networks considered are LIGO Hanford and Livingston (HL); two LIGO detectors and Virgo (HLV); LIGO-Virgo and KAGRA (HLVK) and LIGO-Virgo-KAGRA with LIGO-India (HLVKI). As more detectors are added to the network, the average sensitivity to the second polarization increases. The right plot shows results for the Einstein Telescope (ET), which is comprised of three 60-degree interferometers, ET and three LIGO-Voyager detectors (Voyager-ET) and ET with either one or two Cosmic Explorer detectors (1CE-ET and 2CE-ET). Here, $\widetilde{\alpha}$ represents the mean value of α for the given detector network. As the ET detector has good sensitivity to both polarizations, networks where ET is the most sensitive detector will have large values of α. Third generation target noise curves are taken from [80].
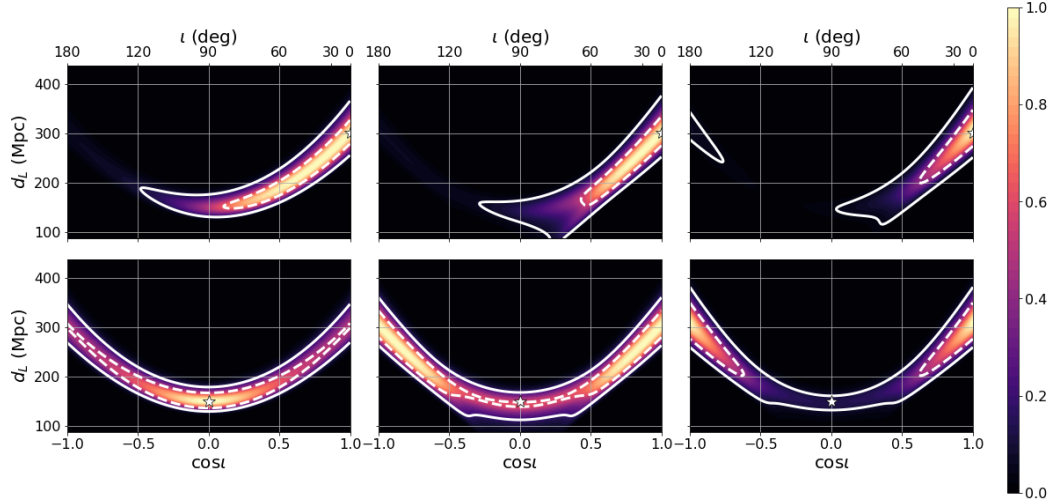
Figure 2.4: The progression of the probability distributions over a $\cos\iota$ and distance parameter space for a signal detected with alignment factor $\alpha = 0.1$ and signal to noise ratio $\rho = 12$. The top panel shows the distribution for an face-on signal. The bottom panel shows the distribution for an edge-on signal. The leftmost plots are the distribution for *only* the likelihood. The middle plots show the distribution after we have marginalized over a flat prior for ϕ and ψ. Lastly, the rightmost plots are the complete probability distribution, calculated by applying a distance-squared weighting to the likelihood. This is to account for the expectation that binary systems are distributed uniformly in volume. Recall that $\alpha = 0.1$ is the mode sensitivity for the Hanford-Livingston network. The white star represents the hypothetical signal. The white contours represent the 50% and 90% confidence intervals obtained from our simplified model. Note that these contours do not represent the results of full parameter estimation, as they did in Figure 2.1. From these plots, we can see that at this α, a side-on signal is indistinguishable from a face-on/face-away signal.
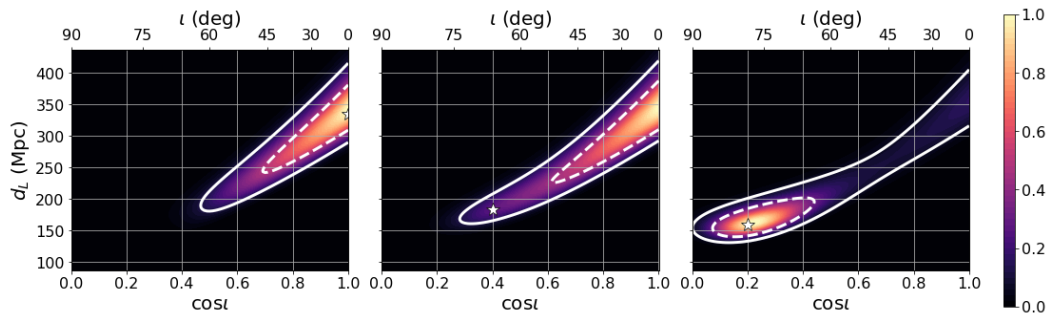
Figure 2.5: The probability distribution over a $\cos \iota$ and distance parameter space for a signal detected with alignment factor $\alpha = 0.5$ and signal to noise ratio $\rho = 12$. The white star represents the injected signal. The white contours represent the 50% and 90% confidence intervals obtained from our simplified model. Note that these contours do not represent the results of full parameter estimation, as they did in Figure 2.1. A face-on signal (where $\cos \iota = 1$) returns a nearly identical probability distribution of the parameter space as a signal from a binary with an inclination of about 66 degrees ($\cos \iota = 0.4$). For inclinations in the range $0.1 < \cos \iota < 0.4$, though the distribution now peaks at the correct inclination, there is support extending across from face-on to an inclination of $\iota \sim 80° - 90°$. In these cases it is not possible to distinguish the binary inclination. The signal is only clearly identified as *not* face-on after $\cos \iota < 0.1$.
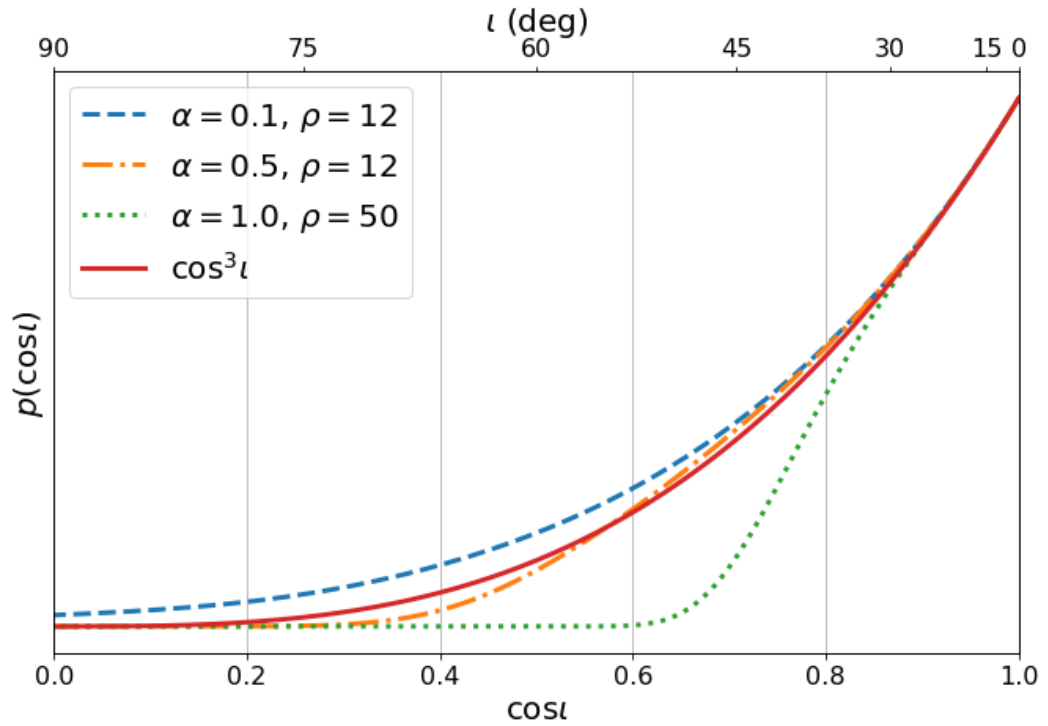
Figure 2.6: The un-normalized marginalized posterior for $\cos\iota$ for a face-on source as measured for three networks with alignment factors $\alpha = 0.1$, $\alpha = 0.5$, $\alpha = 1.0$ and signal to noise ratio $\rho = 12$, $\rho = 12$, $\rho = 50$ respectively. The solid line shows the expected $\cos^3\iota$ form of the likelihood.
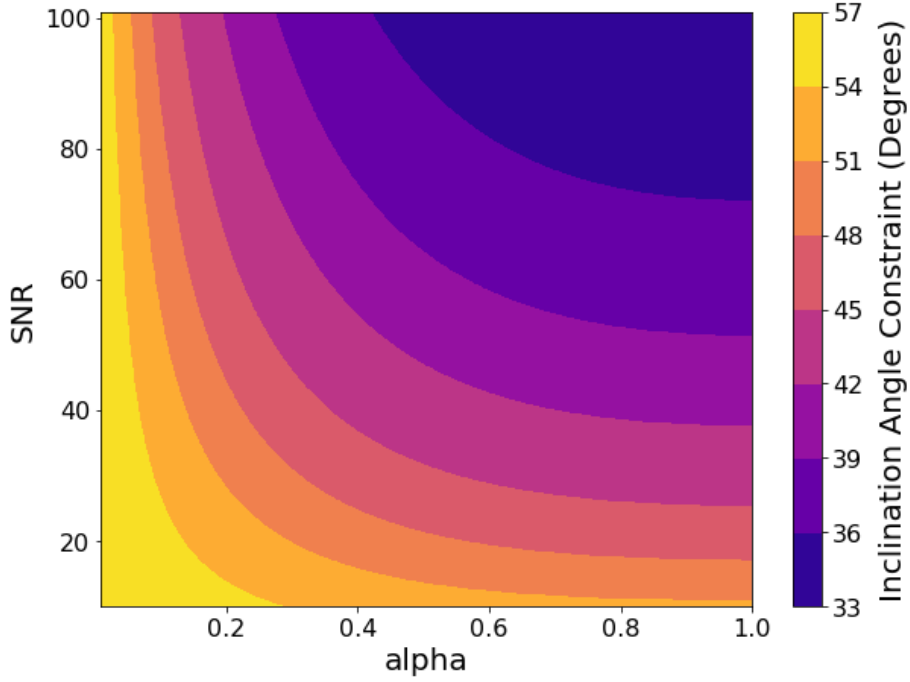
Figure 2.7: This plot shows a detector network's ability to constrain the inclination of a face-on signal with 90% confidence. The x-axis shows the network alignment factor α, whereas the y-axis shows the signal-to-noise ratio (SNR) of the hypothetical gravitational-wave signal. The colour represents the upper limit on the inclination angle. For weak signals or for networks which are not very sensitive to the cross polarization, the network can only constrain the inclination to being less than about 45°. Even for the most sensitive detector network detecting the loudest hypothetical signals, the network would be unable to constrain the inclination to being less than 30°. However, we note that at these SNRs, the detector network may be able to identify higher order modes, which would break the degeneracy between distance and inclination and allowing us to constrain the inclination more precisely.
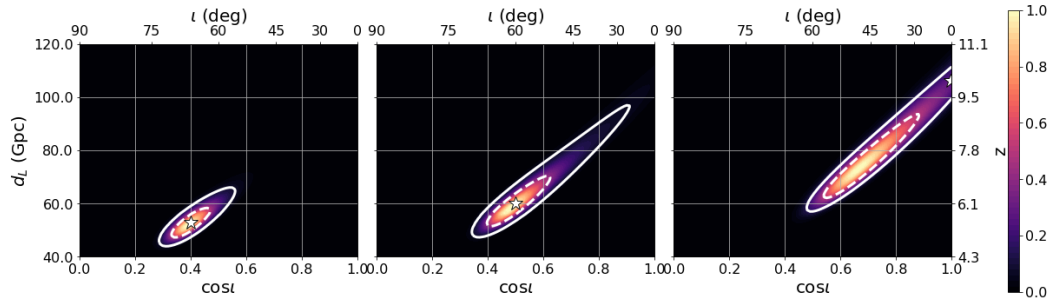
Figure 2.8: Marginalized posterior distribution for a $10M_\odot - 10M_\odot$ binary black hole at redshift $z = 10$ detected by the Einstein Telescope in the most sensitive part of the sky, i.e. directly above the detector. Here, the alignment factor is $\alpha = 1$ and the signal-to-noise ratio is $\rho = 20$. The white star represents the injected signal at three different inclinations: $\iota = 66°$, $\iota = 60°$ and $\iota = 0°$. The white contours represent the 50% and 90% confidence intervals obtained from our simplified model. Note that these contours do not represent the results of full parameter estimation, as they did in Figure 2.1. We use a prior that is a uniform in comoving volume with a rest frame rate density that follows the star formation rate [65]. At this redshift the prior varies by a factor of ~ 12 across the degeneracy and now favours more inclined binaries. Thus binaries that are face-on will be recovered as being more inclined. The redshift uncertainty $\Delta z / z \sim 40\%$ dominates the statistical error in the recovery of the binary chirp mass. All conversions between luminosity distance and redshift assume standard cosmological parameters [82].

Chapter 3

Overview of the Search Pipeline

To identify gravitational waves in LIGO's noisy data, we use a sophisticated search workflow to process the data. The main takeaway from this pipeline is the best-matched gravitational-wave template. However, lots of information could be used for parameter estimation. Because of this, our parameter estimation analysis is based on and uses information from the gravitational-wave search pipeline PyCBC. We explain the basic setup of this analysis so that the setup for our parameter estimation pipline is clear. More details of the offline search pipeline can be found in [24].

3.1   Template Bank and Match Filtering

Gravitational waves have amplitudes comparable to the noise background in the LIGO detectors, but gravitational waves from binary star systems can be well-modeled using analytic and numerical methods. This implies that match filtering is a useful method of identifying gravitational waves amongst the detector noise. The search pipeline thus uses a set of predicted gravitational waveforms called a *template bank* which is used to compare to the data set using a match filter. This bank is usually very large, covering the entire target parameter space and containing thousands of templates. Each template is individually match filtered against the data. This filtering algorithm is:

$$(s|h)(t) = 4\text{Re} \int_{f_{\text{low}}}^{f_{\text{high}}} \frac{\tilde{s}(f)\tilde{h}^*(f)}{S_n(f)} e^{2\pi i f t} \, \mathrm{d}f. \tag{3.1}$$

This equation is effectively a weighted dot product and tells us if a template waveform, h, is a significant component in the detector data, s, given the detector noise $S_n(f)$, over the sensitive band of frequencies (from f_{low} to f_{high}).

When you divide by the magnitude of the waveform, $\sqrt{(h|h)}$, the result is called the signal-to-noise ratio, or *SNR*, and is denoted ρ. By repeating this calculation at every data point, the pipeline creates an SNR timeseries, which describes the match between the template waveform and the data over time. We also maximize over the phase of the signal. Each template waveform has two orthogonal phases, h_0 and $h_{\frac{\pi}{2}}$. The resulting match filter is:

$$\rho^2(t) = \frac{(s|h_0)^2}{(h_0|h_0)} + \frac{(s|h_{\frac{\pi}{2}})^2}{(h_{\frac{\pi}{2}}|h_{\frac{\pi}{2}})} = \frac{(s|h_0)^2 + (s|h_{\frac{\pi}{2}})^2}{(h_0|h_0)} \tag{3.2}$$

Any template with an SNR higher than a predetermined threshold are flagged as *triggers* and undergo additional statistical testing, as is explained in Section 3.2. The finer details of this matched filtering are explained in [24].

The template bank used in the search is designed so that any gravitational wave within the parameter space of the the search would be at least 97% similar to one of the gravitational wave templates. This threshold is called the *minimum match* and can be adjusted. The minimum match thus determines how tightly packed the template bank needs to be when it is generated. The more similar the template is to the gravitational-wave template, the higher the SNR. However, a higher minimum match would increase the number of templates in the bank, thus increasing the computational cost of the search and slowing down the analysis. Setting the minimum match to 97% is a good compromise between recovering the most SNR from a signal without burdening the search.

3.2 χ^2 Test

Many statistical tests are performed on the gravitational-wave candidates to verify that they are true signals instead of a noise fluctuation. Arguably the most significant of these is the χ^2 test [90]. This test effectively cuts the predicted waveform into p bins of equal power, then match filters each bin with respect to the data. This is described by the equation:

$$\chi^2 = p \sum_{i=1}^{p} \left[\left(\frac{\rho_0^2}{p} - \rho_{0,i}^2 \right)^2 + \left(\frac{\rho_{\frac{\pi}{2}}^2}{p} - \rho_{\frac{\pi}{2},i}^2 \right)^2 \right]. \tag{3.3}$$

This test measures if the power distribution of a gravitational-wave candidate matches what we expect from the data, given the predicted waveform. If the distribution is similar, it will return a number between zero and one, with a

dissimilar distribution returning a high number and random noise returning a number near unity. For candidates that return a χ^2 statistic greater than one, the candidate's SNR is downweighted by:

$$\hat{\rho} = \frac{\rho}{\left[\frac{1+(\chi_r^2)^3}{2}\right]^{\frac{1}{6}}} \tag{3.4}$$

where $\hat{\rho}$ is the reweighted SNR and $\chi_r^2 = \chi^2/(2p-2)$ is the reduced χ^2 statistic. This reduction comes from the $2p - 2$ degrees of freedom in the χ^2 statistic. This check plays a significant role in removing triggers caused by loud transient noises in the detector matching with template waveforms. The resulting reweighted SNR is then used to determine the significance of the gravitational-wave candidate with respect to the background. Since a gravitational wave may match highly with several different template waveforms, the analysis will choose the loudest candidate within a window as the best-fit waveform for the trigger. Further research to reweight signals is ongoing, including a test similar to the χ^2 test using sine-Gaussian tiles, described in [91].

3.3 Coincidence Testing

Since gravitational waves travel at the speed of light, we expect gravitational waves to be found with the same gravitational-wave template in the two LIGO detectors within the light-travel time between the two detectors. This means that a gravitational wave should reach both detectors within ten milliseconds. In order to account for timing errors, we loosen the restriction to about fifteen milliseconds. This coincidence testing is vital, as it also becomes the basis for generating a set of background triggers, which is created by shifting the timestamps of the gravitational-wave candidates of one detector with respect to the gravitational-wave candidates of the other detector within the light travel time. Any resulting coincidences are therefore a result of noise. These time shifts are described in further detail in [24].

We calculate the final ranking statistic using the coincident signals. After identifying triggers in both detectors and calculating their reweighted SNR using 3.4, we then take the square root of the quatrature sum of the SNRs in each detector:

$$\rho_c = \sqrt{\rho_{H1}^2 + \rho_{L1}^2}, \tag{3.5}$$

where ρ_c is the combined reweighted SNR. This is performed for all coinci-

dences in both the background and foreground. We then compare this detection statistic for the foreground triggers to the detection statistic for the background triggers to calculate the *false-alarm rate*, or *FAR*, for the foreground signals.

Chapter 4

Rapid Parameter Estimation

Our search pipeline allows us to find the very quiet gravitational wave in noisy strain data, as described in Chapter 3. The detectors give a lot of information about the gravitational-wave signal, much of which is, at the moment, discarded. Our aim is to leverage this additional information to improve our rapid parameter estimation analysis. Low-latency parameter estimation are necessary so that we can learn about the parameters of the source binary very quickly. The information we extract can be useful for astronomers to search for an electromagnetic counterpart to a gravitational wave. For any given signal, we have information about the best-fit template, including the template's masses and spins, as well as the time this waveform peaks in the data, its SNR and reweighted SNR at this time, and the time difference between the two detectors. However, the pipeline also keeps information for triggers for all waveforms in the template bank. Using this information would allow us to more quickly and more easily constrain the parameters of the source binary.

4.1   Template Bank Generation

The first step in our parameter estimation code is to generate a bank of template waveforms. From the search, we will know the parameters of the best-fit template in the search pipeline's coarse bank of templates.

We use information from the search to build a more focused, dense bank in the region containing the signal. The pipeline used for the binary search uses the same method of matched filtering template waveforms. In particular, the search uses a large, coarse bank that covers a wide parameter space and matched filters every template against every moment of data in the data set, using Eq. 3.1; Meanwhile, our code uses a small, dense bank of templates fo-

cused only on the area of parameter space surrounding the loudest template found in the search pipeline and matched filters it only against the chunk of data containing the signal, approximately 256 seconds long. Since the template waveforms are not orthogonal, a signal will usually cause multiple templates within a template bank to be flagged as gravitational-wave candidates. The search pipelines will simply take the signal with the loudest SNR as the detected gravitational-wave candidate. However, we can use the information from which templates in the template bank were flagged to tell us more about the detection. From the search, our pipeline loads in the information about which templates were flagged within the one-second window around the time of detection.

We create a bank which covers the 99.9% confidence interval of the original template bank. We calculate this confidence interval by finding the probability for each gravitational-wave template and looking at the probability distribution over the original parameter space.

We can expect the detector $s(t)$ to either contain noise, $n(t)$, or both signal and noise $h(t) + n(t)$ [61]:

$$
s(t) = \begin{cases} h(t) + n(t), & \text{if a signal is present} \\ n(t). & \text{if there is no signal} \end{cases}
$$

Instrumental noise $n(t)$ is a randomly occuring process, and can be described through a probability distribution function. For our argument, we assume the noise is stationary and Gaussian, with a mean value of 0: $\langle n(t) \rangle = 0$. We can write the noise as $n = s - h$. The likelihood of getting noise is simply:

$$
p(n) = e^{-\frac{1}{2}(s-h|s-h)} \tag{4.1}
$$

By Bayesian statistics, the likelihood of getting the signal h given the data s is thus:

$$
\frac{p(s|h)}{p(s|0)} = \frac{e^{-\frac{1}{2}(s-h|s-h)}}{e^{-\frac{1}{2}(s|s)}} \tag{4.2}
$$

For a given waveform h, the probability that the signal h is present in the data is proportional to the likelihood. The log-likelihood for a waveform is simply:

$$
\ln(\Lambda) = (s|h) - \frac{1}{2}(h|h), \tag{4.3}
$$

where $(s|h)$ is defined in Eq. 3.1. This can be interpreted as the component

of the data containing the signal, minus the magnitude of the waveform itself. This formula allows us to focus on the significance of the waveform in the data without being weighted towards waveform which contain more overall power than other waveforms in the set. From here, we can intuitively see that the log-likelihood for a network of detectors is simply the sum of the individual contributions from each detector:

$$\sum_i \ln(\Lambda_i) = (s|h) - \frac{1}{2}(h|h), \tag{4.4}$$

where $(a|b) = \sum_i (a_i|b_i)$.

We can then use the SNR of a template to find its likelihood. Our parameter estimation code focuses on analyzing data which we know contains a gravitational wave from the initial analysis. For this reason, the inital information we receive will use reweighted SNR, but our parameter estimation analysis will focus specifically on the unweighted SNR. Similarly, our parameter estimation code is meant to be run on triggers that have already been determined to be true signals, therefore we do not use time slides for background estimation. Once calculated for all templates in our parameter space, we can use the likelihoods to estimate the probability distribution over the space.

We want to maximize the likelihood over amplitude. If we assume the signal h has an unknown amplitude A for a single polarization h_0, $h = Ah_0$, then

$$\ln \Lambda = (s|h) - \frac{1}{2}(h|h) = A(s|h_0) - \frac{A^2}{2}(h_0|h_0). \tag{4.5}$$

To find the peak amplitude, we take the derivative with respect to A and set it to zero, and solve for A:

$$\frac{\partial}{\partial A}\left[A(s|h_0) - \frac{A^2}{2}(h_0|h_0) \right] = 0, \tag{4.6}$$

which gives:

$$A = \frac{(s|h_0)}{(h_0|h_0)}. \tag{4.7}$$

This simplifies our log-likelihood equation to simply the SNR squared over 2:

$$\ln \Lambda = \frac{(s|h_0)^2}{2(h_0|h_0)} = \frac{\rho^2}{2} \tag{4.8}$$

Therefore, from the SNRs of each template, we can find the likelihood for

each flagged template i using:

$$p_i \propto e^{\frac{\rho_i^2}{2}}.$$ (4.9)

We sum up these probabilities for every waveform i and then divide each probability by this normalization factory. When normalized, this equation then becomes:

$$p_i = \frac{e^{\frac{\rho_i^2}{2}}}{\sum_j e^{\frac{\rho_j^2}{2}}}$$ (4.10)

We then order these waveforms by their probability, and sum up the probabilities until we get the total probability we would like in our interval. For our analysis, we chose the 99.9% confidence interval. Then we look at the template waveforms contained in the interval and use it to define the edges of our hyperdense bank. By summing up these probabilities, we can estimate the 99.9% confidence interval for the signals in the coarse bank.

This 99.9% confidence interval then becomes our bounds for the hyperdense bank in the parameter estimation code. We take the smallest and largest values of the individual masses m_1 and m_2, the chirp mass $\mathcal{M}_{chirp} = \frac{(m_1 m_2)^{\frac{3}{5}}}{(m_1+m_2)^{\frac{1}{5}}}$, the individual spins χ_1 and χ_2 and the effective spin $\chi_{eff} = \frac{\chi_1 m_1 + \chi_2 m_2}{m_1 + m_2}$ and later use these as the lower and upper bounds over the mass-spin parameter space.

Next, we create a grid of points with a fixed step in each direction (determined by the desired minimum match of the bank) over this parameter space. Using a uniformly spaced grid allows us to sample the parameter space in a simple and intuitive way without biasing our search to any particular region of the bank which would be more or less covered if we were using a different placement such as the stochastic bank method [92]. To determine the grid spacing, we take the loudest signal from the search and generate a template nearby in the parameter space and test the match between the two waveforms. We can expect the match to fall off roughly quadratically as we move away from the peak match in parameter space [93]. This allows us to estimate how quickly the signals become dissimilar as we move through this dimension of the parameter space. If a waveform is matched with itself, the match will return 1. Because of this, we know that the form of the match fall off will be $m = 1 - k\Delta\lambda^2 + 1$ where $\Delta\lambda$ is the change in one of the parameters and m is the match between the old and the new waveform, for some constant k. If we generate a waveform whose bigger object has mass is $M_0 M_\odot$ larger than our original waveform and returns a match of m_0, we can rewrite our equation to

find the rate of fall off, k:

$$k = \frac{m_0 - 1}{\mathrm{M}_0^2} \tag{4.11}$$

which can be plugged into the original match as:

$$\mathrm{m}_0 = \left(\frac{m_0 - 1}{\mathrm{M}_0^2} \right) \Delta M^2 \tag{4.12}$$

We can set m equal to the match we would like between the waveforms in our bank, D, and solve for the necessary change in the parameters $\Delta \lambda$ to get the correct grid spacing:

$$\Delta \Lambda = \mathrm{M}_0 \sqrt{\frac{1 - D}{1 - m_0}} \tag{4.13}$$

Since the fall off of the match is only approximately quadratic, we use a loop to repeat this calculation by generating a waveform with the newly calculated difference in the parameter space. This is repeated until the change in match is within a small range of what we want for the gridding.

Once the grid of points in the parameter space has been generated, we cull the points outside of the 99.9% confidence interval from the search, as described earlier. Since the spacing is estimated in both mass parameters and both spin parameters, the bank generated is well-covered in the region of the parameter space containing the signal, without biasing our search. We also limited our spins to having a magnitude less than 0.98, since attempting to match filter with a spin greater than 0.98 caused the code to fail. You can see the result of this in Figure 4.1.

This template bank presented some limitations when running on a single-core computer. For example, a bank at this density in all four dimensions of this parameter space (two dimensions for mass parameters and two for spin parameters) has far too many templates to run quickly on a single computer. One solution for this issue would be to confiugre the code so it could run on a network of computers. In addition, the grid of points is laid out linearly in the parameter space. The method of placement could be further explored to allow for a more efficient placement method.

4.2 Match Filtering

Next, our hyperdense parameter estimation pipeline uses the same matched-filtering as used in the PyCBC pipeline, Eq. 3.1, to find the significance of the waveforms in the hyperdense template bank. We then take the loudest signal-
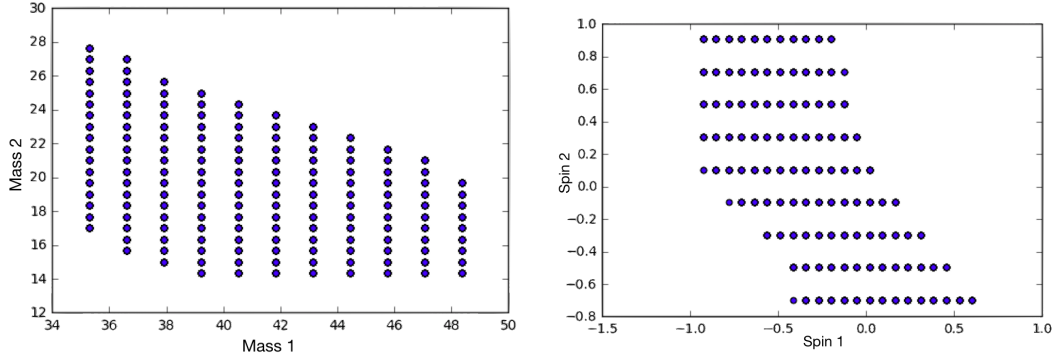
Figure 4.1:   An example hyperdense bank for the gravitational wave GW170104, spanning the four-dimensional mass-spin parameter space. The left plot shows the bank in the mass parameter space in solar masses, where the x-axis is mass 1, the bigger black hole's mass, and the y-axis is mass 2, the smaller black hole's mass. The right plot shows the bank in the spin parameter space, where x-axis is spin 1, the spin of the bigger black hole, and the y-axis is spin 2, the spin for the bigger mass.

to-noise ratio for each template within the one-second interval around the reported end time. The fall off of the SNRs over the parameter space tells us the likely range for the signal's parameters. We calculate the 99.9% confidence interval for the returned SNRs and use it to approximate the masses and spins of the signal. This method of matched filtering for points over the parameter space is related to other parameter estimation pipelines' method of randomly walking over the parameter space (often using a Markov-Chain Monte Carlo) insofar that both methods sample the parameter space at different points to estimate the overall structure of the probablities.

Thus, we use Eq. 3.1 to match every waveform in our template bank against the 256 s segment of data in which the gravitational-wave signal was identified by the pipeline. Recall that this uses the noise in the detector to weight the matched filter. We thus Fourier transform the data segment to generate a power spectral density for the matched filter. This allows us to downweight excess power from noisy frequecies, such as the low-frequency seismic noise or the high-frequency photon shot noise discussed in Section 1.3. Note that Eq. 3.1 is a timeseries: the output gives the SNR for a given waveform over the course of the time segment. We know the approximate time of the signal (defined as the point of merger in the waveform) from the search, so we find the peak value of the SNR in a one-second window around this time for each template waveform. These peak values, the time stamp and the parameters of the template waveform are saved in a database. This process is done for each contributing gravitational-wave detector.

We then weight the SNR to account for the astrophysical distribution of sources, ϕ. This factor is found by consulting an empirically calculated table. This table is generated by creating a set of simulated gravitational-wave sources which are uniform in volume. For each of these hypothetical sources, the associated SNR and phase for each detector is calculated, along with the time difference between detectors. Then we histogram over these parameters to find the probability of expected signals over this space. This probability is then used to reweight the SNR in order to favor signals that are more astrophysically likely. This is described in detail in Ref. [94].

4.3 Sky Rings

Next, we then need to calculate the combined likelihood statistic. For our research, we focused on an analysis of the Hanford and Livingston detectors only, so we need only find the combined statistic between the events found in these two data sets. We calculate the constants for each signal including time delay, the amplitude of the gravitational waveform σ, maximum distance and the combined SNR squared ρ^2. Next we use a relatively new method of calculating the sky location to make further calculations, using sky rings. Using the SNRs from the matched filtering process and the difference in the time delays, we can also estimate the sky location and orientation of the binary system.

We generate a set of rings of points at different sky locations. These rings are generated such that a gravitational wave coming from a sky location on any point along a single ring would have the same time delay when detected by the Hanford and Livingston detectors. In order to generate these rings, we need the time-of-arrival for the gravitational wave. We feed this information from the search. We convert this to Greenwich mean sidereal time. We then create a line of maximum time delay, which is the line that runs through Hanford and Livingston. This line points to two sky locations from which a gravitational wave would give the maximum possible time delay between the detectors. This maximum time delay is equal to the light travel-time between detectors, about 11 ms, since gravitational waves travel at the speed of light. Next we generate rings in the sky centered along the line of maximum time delay. For our analysis we choose 180 rings of 300 points. We can then calculate the detector response, F_+ and $F_\times$, for each of these sky points. For each waveform, once the match filter is performed, the difference in the end times between the two

detectors constrains the signal to the ring of points with the most similar time delay.

We can use these sky rings to identify the orientation of the binary. Using the detector response for each of the sky points, we can see if the observed SNRs are consistent with the signal. If the components of the flagged gravitational wave are similar to the response we expect to see in the detector, the signal is more likely to have come from that sky point. Similarly, we can use the detector response at each sky point to find how the signal's SNR can be attributed to being face-on, face-away or edge-on. As discussed in detail in Chapter 2, face-on and face-away binaries are more likely to be detected. We quantify this by calculating the SNRs weighted by the expected detector response:

$$\rho_{right} = \left| \frac{z_H F_H \sigma_H + z_L F_L \sigma_J}{\sqrt{\sigma_H^2 F_H^2 + \sigma_L^2 F_L^2}} \right| \tag{4.14}$$

$$\rho_{left} = \left| \frac{z_H \bar{F}_H \sigma_L + z_L \bar{F}_L \sigma_L}{\sqrt{\sigma_H^2 F_H^2 + \sigma_L^2 F_L^2}} \right| \tag{4.15}$$

Here, z_H and z_L are the complex SNR values for Hanford and Livingston, respectively. σ is the norm of the gravitational waveform. F is the detector response to the components of the signal for each detector, e.g., $F_H = F_{H,+} + iF_{H,\times}$, while $\bar{F}$ is its conjugate. We can also estimate the SNR for an edge-on binary as being the norm of the complex SNRs in the two detectors.

$$\rho_{coherent} = |z_H|^2 + |z_L|^2. \tag{4.16}$$

From these SNRs, we can calculate the approximate distance of the binary. Since a nearby binary would create the loudest signal, the distance is inversely proportional to the signal's SNR:

$$d = \frac{\sigma}{\rho}. \tag{4.17}$$

We calculate this for each waveform, at each point, for face-on, face-away and edge-on orientations.

Once we have all the SNRs for the three orientations for each waveform at each point on its optimum sky ring, we can calculate the probabilities for each of these points (as used in Eq. 4.1). We sum the probabilities for all waveforms at each point to find which location is most likely for our newly generated bank. We also sum the probabilities for each handedness to find if

the binary was likely to be face-on or edge-on. Lastly, we do a weighted sum to determine what the distance is most likely to be.

4.4   Confidence Regions

After calculating the signal-to-noise ratio at the time of the detection for each waveform, we use Eq. 4.1 to estimate the probabilites for each waveform. Using these probabilities, we generate 90% and 50% confidence intervals for each part of the parameter space. We do this by organizing the templates by their probabilities, and then totaling the probabilities until we reach a cumulative probability of 90% and 50%, respectively, as is done for the coarse bank in Sec. 4.1.

4.5   Discussion and Future Direction

Here, we present an exploration into a new method for rapid parameterization. This parameter estimation pipeline has been tested on the gravitational-wave signal GW170104, and is able to approximate the masses, spins, distance, inclination and sky location on the order of hours for a single-core computer. The method works in principle, though several changes need to be made in order to optimize the method for use in the collaboration. For example, the density of the bank made it difficult to run on a small scale. If this were to be expanded to running for multiple detections over the course of a observing run, it may be computationally expensive to perform this parameter estimation. By finding a better way to uniformly cover the mass space, such as placing the templates diagonally and optimizing the spacing between templates in the parameter space, we could minimize the run time. It may also be possible to create a single, large hyperdense bank and use the boundaries defined in Sec. 4.1 to cull this bank for the parameter estimation analysis. Secondly, this code would be best used to run automatically when low-latency pipelines identify a significant signal in the gravitational-wave data. This requires creating a code which merges seamlessly with one of the already existing low-latency pipelines such as PyCBCLive [30].

Chapter 5

Conclusions

In this thesis, I have presented my work in gravitational waves over the past two years. This research focused on parameter estimation of binary systems using the resulting gravitational wave. I explored LIGO's parameter estimation in Chapter 2. Here, I found that current LIGO would rarely be able to correctly constrain the inclination angle for most binary signals, due to the degeneracy between distance and inclination. Future detector networks may be able to constrain the face-on signals to having less than about $45°$, but it would be difficult to constrain it more tightly than that without breaking degeneracy by measuring distance using an EM counterpart, by measuring precession effects or by detecting higher order modes. I give details on the overview of the search pipelines currently used to identify gravitational waves in LIGO data in Chapter 3, which was a significant component of my undergraduate research. This work I completed and published during my first months in Cardiff [24]. This gave the background necessary to understand the parameter estimation work I performed, which I described in detail in Chapter 4. This novel parameter estimation pipeline has been tested to work, but would need significant optimization in order to be implemented in LIGO research. This work could be used to help our astronomer colleagues to better understand what type of signal they may be looking for associated with a gravitational wave.

Bibliography

[1] B. Abbott et al. LIGO: The Laser Interferometer Gravitational-Wave Observatory. *Rept. Prog. Phys.*, 72:076901, 2009.

[2] T. Accadia et al. Virgo: a laser interferometer to detect gravitational waves. *JINST*, 7:P03012, 2012.

[3] B. P. Abbott et al. Observation of Gravitational Waves from a Binary Black Hole Merger. *Phys. Rev. Lett.*, 116(6):061102, 2016.

[4] B. P. Abbott et al. GW151226: Observation of Gravitational Waves from a 22-Solar-Mass Binary Black Hole Coalescence. *Phys. Rev. Lett.*, 116(24):241103, 2016.

[5] Benjamin P. Abbott et al. GW170104: Observation of a 50-Solar-Mass Binary Black Hole Coalescence at Redshift 0.2. *Phys. Rev. Lett.*, 118(22):221101, 2017.

[6] B. P. Abbott et al. GW170814: A Three-Detector Observation of Gravitational Waves from a Binary Black Hole Coalescence. *Phys. Rev. Lett.*, 119(14):141101, 2017.

[7] B.. P.. Abbott et al. GW170608: Observation of a 19-solar-mass Binary Black Hole Coalescence. *Astrophys. J.*, 851(2):L35, 2017.

[8] B. P. Abbott et al. On the Progenitor of Binary Neutron Star Merger GW170817. *Astrophys. J.*, 850(2):L40, 2017.

[9] Vladimir Lipunov, Victor Kornilov, Evgeny Gorbovskoy, Galina Lipunova, Daniil Vlasenko, Ivan Panchenko, Nataly Tyurina, and Valery Grinshpun. The discovery of the neutron stars merger GW170817/GRB170817A and a binary stars evolution. *New Astron.*, 63:48–60, 2018.

[10] V. M. Lipunov, K. A. Postnov, and M. E. Prokhorov. Formation and coalescence of relativistic binary stars: effect of kick velocity. *Mon. Not. Roy. Astron. Soc.*, 288:245, 1997.

[11] Remya Nair, Sukanta Bose, and Tarun Deep Saini. Measuring the Hubble constant: gravitational wave observations meet galaxy clustering. 2018.

[12] Soumi De, Daniel Finstad, James M. Lattimer, Duncan A. Brown, Edo Berger, and Christopher M. Biwer. Constraining the nuclear equation of state with GW170817. 2018.

[13] Isaac Newton. Newton's principia : The mathematical principles of natural philosophy. 1845.

[14] V. K. Shchigolev. Analytical Computation of the Perihelion Precession in General Relativity via the Homotopy Perturbation Method. *J. Comput. Math.*, 3:45–49, 2015.

[15] R. Abuter et al. Detection of the gravitational redshift in the orbit of the star S2 near the Galactic centre massive black hole. 2018.

[16] Albert Einstein. Grundlage der allgemeinen relativittstheorie. *Annalen der Physik*, 49:769–822.

[17] Albert Einstein. Nherungsweise integration der feldgleichungen der gravitation. *Preussische Akademie der Wissenschaften, Sitzungsberichte*, page 688696, 1916.

[18] Laura Nuttall. *Electromagnetic Follow-Up of Gravitational Wave Candidates*. PhD thesis, Cardiff University, 2013.

[19] Laura Nuttall. *Electromagnetic Follow-Up of Gravitational Wave Candidates*. PhD thesis, Cardiff University, 5 2013.

[20] B. P. Abbott et al. GW150914: The Advanced LIGO Detectors in the Era of First Discoveries. *Phys. Rev. Lett.*, 116(13):131103, 2016.

[21] J. Aasi et al. Advanced LIGO. *Class. Quant. Grav.*, 32:074001, 2015.

[22] F. Acernese et al. Advanced Virgo: a second-generation interferometric gravitational wave detector. *Class. Quant. Grav.*, 32(2):024001, 2015.

[23] Beverly Berger. Tracking down the origins of advanced ligo noise: some examples. LIGO Scientific Collaboration, 4 2018. Presentation given at American Physical Society.

[24] Samantha A. Usman et al. The PyCBC search for gravitational waves from compact binary coalescence. *Class. Quant. Grav.*, 33(21):215004, 2016.

[25] Iair Arcavi et al. Optical emission from a kilonova following a gravitational-wave-detected neutron-star merger. *Nature*, 551:64, 2017.

[26] E. Troja et al. The X-ray counterpart to the gravitational wave event GW 170817. *Nature*, 551:71–74, 2017. [Nature551,71(2017)].

[27] Brian D. Metzger. Welcome to the Multi-Messenger Era! Lessons from a Neutron Star Merger and the Landscape Ahead. 2017.

[28] LIGO-P1800061-v9: Properties of the binary neutron star merger GW170817, 2018.

[29] Alexei Pozanenko, Maxim V. Barkov, Pavel Yu Minaev, Alina A. Volnova, Elena D. Mazaeva, Alexander S. Moskvitin, Maxim A. Krugov, Vladimir A. Samodurov, Vladimir M. Loznikov, and Maxim Lyutikov. GRB170817a associated with GW170817: multifrequency observations and modeling of prompt gamma-ray emission. *arXiv:1710.05448 [astro-ph]*, October 2017. arXiv: 1710.05448.

[30] Alexander H. Nitz, Tito Dal Canton, Derek Davis, and Steven Reyes. PyCBC Live: Rapid Detection of Gravitational Waves from Compact Binary Mergers. 2018.

[31] Will M. Farr, Simon Stevenson, M. Coleman Miller, Ilya Mandel, Ben Farr, and Alberto Vecchio. Distinguishing Spin-Aligned and Isotropic Black Hole Populations With Gravitational Waves. *Nature*, 548:426, 2017.

[32] Javier Roulet and Matias Zaldarriaga. Constraints on Binary Black Hole Populations from LIGO-Virgo Detections. 2018.

[33] Bernard Schutz. Gravitational wave astronomy and cosmology. In *Gravitational Wave Astronomy and Cosmology*. LIGO Scientific Collaboration, Royal Astronomical Society, 5 2018. Presentation give at Royal Astronomical Society Meeting on 11 May 2018. LIGO Document G1800946.

[34] J. Clark, H. Evans, S. Fairhurst, I. W. Harry, E. Macdonald, D. Macleod, P. J. Sutton, and A. R. Williamson. Prospects for joint gravitational wave and short gamma-ray burst observations. *Astrophys. J.*, 809(1):53, 2015.

[35] A. Goldstein, P. Veres, E. Burns, M. S. Briggs, R. Hamburg, D. Kocevski, C. A. Wilson-Hodge, R. D. Preece, S. Poolakkil, O. J. Roberts, C. M. Hui, V. Connaughton, J. Racusin, A. von Kienlin, T. Dal Canton, N. Christensen, T. Littenberg, K. Siellez, L. Blackburn, J. Broida, E. Bissaldi, W. H. Cleveland, M. H. Gibby, M. M. Giles, R. M. Kippen, S. McBreen, J. McEnery, C. A. Meegan, W. S. Paciesas, and M. Stanbro. An Ordinary Short Gamma-Ray Burst with Extraordinary Implications: Fermi -GBM Detection of GRB 170817a. *The Astrophysical Journal Letters*, 848(2):L14, 2017.

[36] N.R. Tanvir, A.J. Levan, A.S. Fruchter, J. Hjorth, K. Wiersema, et al. A "kilonova" associated with short-duration gamma-ray burst 130603B. *Nature*, 500:547–549, 2013.

[37] V. Ashley Villar, James Guillochon, Edo Berger, Brian D. Metzger, Philip S. Cowperthwaite, Matt Nicholl, Kate D. Alexander, Peter K. Blanchard, Ryan Chornock, Tarraneh Eftekhari, Wen-fai Fong, Raffaella Margutti, and Peter K. G. Williams. The Complete Ultraviolet, Optical, and Near-Infrared Light Curves of the Kilonova Associated with the Binary Neutron Star Merger GW170817: Homogenized Data Set, Analytic Models, and Physical Implications. *arXiv:1710.11576 [astro-ph]*, October 2017. arXiv: 1710.11576.

[38] Samaya Nissanke, Daniel E. Holz, Scott A. Hughes, Neal Dalal, and Jonathan L. Sievers. Exploring short gamma-ray bursts as gravitational-wave standard sirens. *The Astrophysical Journal*, 725(1):496–514, December 2010. arXiv: 0904.1017.

[39] Bernard F. Schutz. Networks of gravitational wave detectors and three figures of merit. *Classical and Quantum Gravity*, 28(12):125023, 2011.

[40] Michele Cantiello, J. B. Jensen, J. P. Blakeslee, E. Berger, A. J. Levan, N. R. Tanvir, G. Raimondo, E. Brocato, K. D. Alexander, P. K. Blanchard, M. Branchesi, Z. Cano, R. Chornock, S. Covino, P. S. Cowperthwaite, P. D'Avanzo, T. Eftekhari, W. Fong, A. S. Fruchter, A. Grado, J. Hjorth, D. E. Holz, J. D. Lyman, I. Mandel, R. Margutti, M. Nicholl,

V. A. Villar, and P. K. G. Williams. A Precise Distance to the Host Galaxy of the Binary Neutron Star Merger GW170817 Using Surface Brightness Fluctuations. *The Astrophysical Journal*, 854(2):L31, February 2018. arXiv: 1801.06080.

[41] Ilya Mandel. The orbit of GW170817 was inclined by less than 28 degrees to the line of sight. *The Astrophysical Journal*, 853(1):L12, January 2018. arXiv: 1712.03958.

[42] Daniel Finstad, Soumi De, Duncan A. Brown, Edo Berger, and Christopher M. Biwer. Measuring the viewing angle of GW170817 with electromagnetic and gravitational waves. *arXiv:1804.04179 [astro-ph, physics:gr-qc]*, April 2018. arXiv: 1804.04179.

[43] The LIGO Scientific Collaboration and the Virgo Collaboration. Properties of the binary neutron star merger GW170817. *arXiv:1805.11579 [astro-ph, physics:gr-qc]*, May 2018. arXiv: 1805.11579.

[44] C. Guidorzi, R. Margutti, D. Brout, D. Scolnic, W. Fong, K. D. Alexander, P. S. Cowperthwaite, J. Annis, E. Berger, P. K. Blanchard, R. Chornock, D. L. Coppejans, T. Eftekhari, J. A. Frieman, D. Huterer, M. Nicholl, M. Soares-Santos, G. Terreran, V. A. Villar, and P. K. G. Williams. Improved constraints on H0 from a combined analysis of gravitational-wave and electromagnetic emission from GW170817. *The Astrophysical Journal*, 851(2):L36, December 2017. arXiv: 1710.06426.

[45] D G Blair, P Barriga, A F Brooks, P Charlton, D Coward, J-C Dumas, Y Fan, D Galloway, S Gras, D J Hosken, E Howell, S Hughes, L Ju, D E McClelland, A Melatos, H Miao, J Munch, S M Scott, B J J Slagmolen, P J Veitch, L Wen, J K Webb, A Wolley, Z Yan, and C Zhao. The Science benefits and preliminary design of the southern hemisphere gravitational wave detector AIGO. *Journal of Physics: Conference Series*, 122:012001, 2008.

[46] Yoichi Aso, Yuta Michimura, Kentaro Somiya, Masaki Ando, Osamu Miyakawa, Takanori Sekiguchi, Daisuke Tatsumi, and Hiroaki Yamamoto. Interferometer design of the KAGRA gravitational wave detector. *Phys. Rev.*, D88(4):043007, 2013.

[47] BS Sathyaprakash, S Fairhurst, BF Schutz, J Veitch, S Klimenko, Dave Reitze, and Stan Whitcomb. Scientific benefits of moving one of LIGO Hanford detectors to India. Technical report.

[48] Daniel Williams, James A. Clark, Andrew R. Williamson, and Ik Siong Heng. Constraints On Short, Hard Gamma-Ray Burst Beaming Angles From Gravitational Wave Observations. *arXiv:1712.02585 [astro-ph, physics:gr-qc]*, December 2017. arXiv: 1712.02585.

[49] A. R. Williamson, C. Biwer, S. Fairhurst, I. W. Harry, E. Macdonald, D. Macleod, and V. Predoi. Improved methods for detecting gravitational waves associated with short gamma-ray bursts. *Phys. Rev.*, D90(12):122004, 2014.

[50] Naoki Seto. Prospects of LIGO for constraining inclination of merging compact binaries associated with three-dimensionally localized short-hard GRBs. *Physical Review D*, 75(2):024016, January 2007.

[51] K. G. Arun, Hideyuki Tagoshi, Chandra Kant Mishra, and Archana Pai. Synergy of short gamma ray burst and gravitational wave observations: Constraining the inclination angle of the binary and possible implications for off-axis gamma ray bursts. *Physical Review D*, 90(2), July 2014. arXiv: 1403.6917.

[52] Hsin-Yu Chen, Salvatore Vitale, and Ramesh Narayan. Measuring the viewing angle of binary neutron star mergers. *arXiv:1807.05226 [astro-ph, physics:gr-qc]*, July 2018. arXiv: 1807.05226.

[53] Dragoljub Marković. Possibility of determining cosmological parameters from measurements of gravitational waves emitted by coalescing, compact binaries. *Physical Review D*, 48(10):4738–4756, November 1993.

[54] Hsin-Yu Chen and Daniel E. Holz. Gamma-Ray-Burst Beaming and Gravitational-Wave Observations. *Physical Review Letters*, 111(18), October 2013.

[55] Curt Cutler and Éanna E. Flanagan. Gravitational waves from merging compact binaries: How accurately can one extract the binary's parameters from the inspiral waveform? *Physical Review D*, 49(6):2658–2697, March 1994.

[56] J. Veitch, I. Mandel, B. Aylott, B. Farr, V. Raymond, C. Rodriguez, M. van der Sluys, V. Kalogera, and A. Vecchio. Estimating parameters of coalescing compact binaries with proposed advanced detector networks. *Physical Review D*, 85(10):104045, May 2012.

[57] M. Punturo, M. Abernathy, F. Acernese, B. Allen, N. Andersson, K. Arun, F. Barone, B. Barr, M. Barsuglia, M. Beker, N Beveridge, S. Birindelli, S. Bose, L. Bosi, S. Braccini, C. Bradaschia, T. Bulik, E. Calloni, G. Cella, E. Chassande Mottin, S. Chelkowski, A. Chincarini, J. Clark, E. Coccia, C. Colacino, J. Colas, A. Cumming, L. Cunningham, E Cuoco, S. Danilishin, K. Danzmann, G. De Luca, R. De Salvo, T. Dent, R. Derosa, L. Di Fiore, A. Di Virgilio, M Doets, V. Fafone, P. Falferi, R. Flaminio, J. Franc, F. Frasconi, A. Freise, P. Fulda, J. Gair, G. Gemme, A. Gennai, A Giazotto, K. Glampedakis, M. Granata, H. Grote, G. Guidi, G. Hammond, M. Hannam, J. Harms, D. Heinert, M. Hendry, I Heng, E. Hennes, S. Hild, J. Hough, S. Husa, S. Huttner, G. Jones, F. Khalili, K. Kokeyama, K. Kokkotas, B. Krishnan, M Lorenzini, H. Lück, E. Majorana, I. Mandel, V. Mandic, I. Martin, C. Michel, Y. Minenkov, N. Morgado, S. Mosca, B Mours, H. Müller-Ebhardt, P. Murray, R. Nawrodt, J. Nelson, R. Oshaughnessy, C. D. Ott, C. Palomba, A. Paoli, G Parguez, A. Pasqualetti, R. Passaquieti, D. Passuello, L. Pinard, R. Poggiani, P. Popolizio, M. Prato, P. Puppo, D Rabeling, P. Rapagnani, J. Read, T. Regimbau, H. Rehbein, S. Reid, L. Rezzolla, F. Ricci, F. Richard, A. Rocchi, S Rowan, A. Rüdiger, B. Sassolas, B. Sathyaprakash, R. Schnabel, C. Schwarz, P. Seidel, A. Sintes, K. Somiya, F Speirits, K. Strain, S. Strigin, P. Sutton, S. Tarabrin, J. van den Brand, C. van Leewen, M. van Veggel, C. van den Broeck, A. Vecchio, J. Veitch, F. Vetrano, A. Vicere, S. Vyatchanin, B. Willke, G. Woan, P. Wolfango, and K. Yamamoto. The third generation of gravitational wave observatories and their science reach. *Classical and Quantum Gravity*, 27(8):084007, 2010.

[58] J. Veitch et al. Parameter estimation for compact binaries with ground-based gravitational-wave observations using the LALInference software library. *Phys. Rev.*, D91(4):042003, 2015.

[59] N. Christensen, A. Libson, and R. Meyer. A Metropolis-Hastings routine for estimating parameters from compact binary inspiral events with laser interferometric gravitational radiation data. *Class. Quant. Grav.*, 21:317–330, 2004.

[60] Christian Rover, Renate Meyer, and Nelson Christensen. Bayesian inference on compact binary inspiral gravitational radiation signals in interferometric data. *Class. Quant. Grav.*, 23:4895–4906, 2006.

[61] Michele Maggiore. *Gravitational Waves*. Oxford university press, 2008.

[62] Nelson Christensen and Renate Meyer. Using Markov chain Monte Carlo methods for estimating parameters with gravitational radiation data. *Phys. Rev.*, D64:022001, 2001.

[63] M. V. van der Sluys, C. Roever, A. Stroeer, N. Christensen, Vicky Kalogera, R. Meyer, and A. Vecchio. Gravitational-Wave Astronomy with Inspiral Signals of Spinning Compact-Object Binaries. *Astrophys. J.*, 688:L61, 2008.

[64] Marc van der Sluys, Vivien Raymond, Ilya Mandel, Christian Rover, Nelson Christensen, Vicky Kalogera, Renate Meyer, and Alberto Vecchio. Parameter estimation of spinning binary inspirals using Markov-chain Monte Carlo. *Class. Quant. Grav.*, 25:184011, 2008.

[65] Piero Madau and Mark Dickinson. Cosmic Star-Formation History. *Annual Review of Astronomy and Astrophysics*, 52(1):415–486, 2014.

[66] Collin Capano, Yi Pan, and Alessandra Buonanno. Impact of higher harmonics in searching for gravitational waves from nonspinning binary black holes. *Phys. Rev. D*, 89:102003, May 2014.

[67] Lionel London, Sebastian Khan, Edward Fauchon-Jones, Cecilio García, Mark Hannam, Sascha Husa, Xisco Jiménez Forteza, Chinmay Kalaghatgi, Frank Ohme, and Francesco Pannarale. First higher-multipole model of gravitational waves from spinning and coalescing black-hole binaries. *arXiv:1708.00404 [gr-qc]*, August 2017. arXiv: 1708.00404.

[68] Theocharis A. Apostolatos, Curt Cutler, Gerald J. Sussman, and Kip S. Thorne. Spin-induced orbital precession and its modulation of the gravitational waveforms from merging binaries. *Phys. Rev. D*, 49:6274–6297, Jun 1994.

[69] B. P. Abbott et al. Binary Black Hole Mergers in the first Advanced LIGO Observing Run. *Phys. Rev.*, X6(4):041015, 2016.

[70] LIGO Scientific and Virgo Collaboration. GW170104: Observation of a 50-Solar-Mass Binary Black Hole Coalescence at Redshift 0.2. *Physical Review Letters*, 118(22):221101, June 2017.

[71] The LIGO Scientific Collaboration and the Virgo Collaboration. GW170608: Observation of a 19-solar-mass Binary Black Hole Coalescence. *arXiv:1711.05578 [astro-ph, physics:gr-qc]*, November 2017. arXiv: 1711.05578.

[72] The LIGO Scientific Collaboration and the Virgo Collaboration. GW170814: A Three-Detector Observation of Gravitational Waves from a Binary Black Hole Coalescence. *Physical Review Letters*, 119(14), October 2017. arXiv: 1709.09660.

[73] LIGO Scientific Collaboration. Gw170817: Observation of gravitational waves from a binary neutron star inspiral. *Phys. Rev. Lett.*, 119:161101, Oct 2017.

[74] K. Thorne. *300 years of Gravitation*. Cambridge University Press, 1987.

[75] S. Klimenko, S. Mohanty, M. Rakhmanov, and G. Mitselmakher. Constraint Likelihood analysis for a network of gravitational wave detectors. *Physical Review D*, 72(12), 2005. arXiv: gr-qc/0508068.

[76] Ian Harry and Stephen Fairhurst. A targeted coherent search for gravitational waves from compact binary coalescences. *Physical Review D*, 83(8), 2011. arXiv: 1012.4939.

[77] Cameron Mills, Vaibhav Tiwari, and Stephen Fairhurst. Localization of binary neutron star mergers with second and third generation gravitational-wave detectors. *Physical Review D*, 97(10):104064, May 2018.

[78] Neil J Cornish and Edward K Porter. The search for massive black hole binaries with lisa. *Classical and Quantum Gravity*, 24(23):5729, 2007.

[79] Sukanta Bose, Archana Pai, and Sanjeev V. Dhurandhar. Detection of gravitational waves from inspiraling compact binaries using a network of interferometric detectors. *Int. J. Mod. Phys.*, D9:325–329, 2000.

[80] Benjamin P. Abbott et al. Exploring the Sensitivity of Next Generation Gravitational Wave Detectors. *Classical and Quantum Gravity*, 34(4), 2016.

[81] Stephen Fairhurst. Localization of transient gravitational wave sources: beyond triangulation. *Class. Quant. Grav.*, 35(10):105002, 2018.

[82] Planck Collaboration. Planck 2015 results. XIII. Cosmological parameters. *Astronomy & Astrophysics*, 594:A13, October 2016. arXiv: 1502.01589.

[83] Tomonori Totani. Cosmological Gamma-Ray Bursts and Evolution of Galaxies. *The Astrophysical Journal Letters*, 486(2):L71, September 1997.

[84] Lee Samuel Finn and David F. Chernoff. Observing binary inspiral in gravitational radiation: One interferometer. *Physical Review D*, 47(6):2198–2219, March 1993. arXiv: gr-qc/9301003.

[85] LIGO and Virgo Scientific Collaboration. Properties of the Binary Black Hole Merger GW150914. *Physical Review Letters*, 116(24):241102, 2016.

[86] Salvatore Vitale and Hsin-Yu Chen. Measuring the Hubble Constant with Neutron Star Black Hole Mergers. *Physical Review Letters*, 121(2):021303, July 2018.

[87] Francesco Pannarale, Emanuele Berti, Koutarou Kyutoku, Benjamin D. Lackey, and Masaru Shibata. Aligned spin neutron star-black hole mergers: A gravitational waveform amplitude model. *Physical Review D*, 92(8):084050, October 2015.

[88] Lawrence E. Kidder. Coalescing binary systems of compact objects to (post${)}\^{5/2}$-Newtonian order. V. Spin effects. *Physical Review D*, 52(2):821–847, July 1995.

[89] Vijay Varma, Parameswaran Ajith, Sascha Husa, Juan Calderon Bustillo, Mark Hannam, and Michael Pürrer. Gravitational-wave observations of binary black holes: Effect of nonquadrupole modes. *Physical Review D*, 90(12):124004, December 2014.

[90] Bruce Allen. χ^2 time-frequency discriminator for gravitational wave detection. *Phys. Rev.*, D71:062001, 2005.

[91] Alexander Harvey Nitz. Distinguishing short duration noise transients in LIGO data to improve the PyCBC search for gravitational waves from high mass binary black hole mergers. *Class. Quant. Grav.*, 35(3):035016, 2018.

[92] Nathaniel Indik, K. Haris, Tito Dal Canton, Henning Fehrmann, Badri Krishnan, Andrew Lundgren, Alex B. Nielsen, and Archana Pai. Stochastic template bank for gravitational wave searches for precessing neutron-starblack-hole coalescence events. *Phys. Rev.*, D95(6):064056, 2017.

[93] S. Babak, R. Balasubramanian, D. Churches, T. Cokelaer, and B. S. Sathyaprakash. A Template bank to search for gravitational waves from inspiralling compact binaries. I. Physical models. *Class. Quant. Grav.*, 23:5477–5504, 2006.

[94] Alexander H. Nitz, Thomas Dent, Tito Dal Canton, Stephen Fairhurst, and Duncan A. Brown. Detecting binary compact-object mergers with gravitational waves: Understanding and Improving the sensitivity of the PyCBC search. *Astrophys. J.*, 849(2):118, 2017.